



NTNU  
Norges teknisk-naturvitenskapelige universitet  
Fakultet for naturvitenskap og teknologi  
Institutt for kjemisk prosess teknologi

# **SPECIALIZATION PROJECT 2016**

**TKP 4580**

**PROJECT TITLE:**

**Modeling and Optimization of Polymerization Semi-Batch Reactors for  
Expandable Polystyrene**

---

**By**

**Marlene Louise Lund**

---

**Supervisors for the project:**

**Johannes Jäschke, NTNU  
Peter Singstad, Cybernetica AS**

**Date:**

**December 16<sup>th</sup> 2016**



# Modeling and Optimization of Polymerization Semi-Batch Reactors for Expandable Polystyrene

**Author:** Marlene Louise Lund  
**Supervisors:** Associate Professor Johannes Jäschke, NTNU  
Peter Singstad, Cybernetica AS

Specialization Project  
Trondheim, 16.12.2016  
Department of Chemical Engineering, Process Systems Engineering  
Norwegian University of Science and Technology



## Abstract

This report has been prepared as a part of the Specialization Project (TKP4580), which is a compulsory element of the final year of the M.Sc. degree in Chemical Engineering at the Norwegian University of Science and Technology (NTNU). The project work was done in collaboration with Cybernetica AS as an extension of a summer internship.

The aim of the project was to model a semi-batch reactor for production of expandable polystyrene (EPS), in addition to developing an offline optimization routine. Further, the primary goals of the optimization were to attain an optimal temperature trajectory and initial reactor recipe in order to minimize the batch time and exploit the available cooling capacity.

The developed model was simulated for different temperatures and amounts of chemical initiator and blowing agent (pentane), and it overall demonstrated the correct qualitative behavior in accordance with expectations from polymerization theory. Parameter estimation was performed using logged time-series data from experiments. The overall dynamic behavior of the new model was improved in terms of predicting the measurement dynamics, but the model did not show improvement towards predicting the end product quality.

To indicate the optimal region of isothermal operation, pre-optimization simulations were performed. The optimal point identified from a surface plot of the batch time gave a base case batch time of 198 minutes. The next step in the investigations was to optimize the monomer to initiator ratio, keeping the temperature constant at the optimal temperature from the pre-optimization simulations. The polymerization time obtained from these calculations was 194.1 minutes. Adding constant temperature to the decision variables of the optimization problem resulted in conditions that shortened the batch time with additional 4.6 minutes. Finally, optimizing the monomer to initiator ratio and the temperature trajectory over the batch time horizon gave a significantly reduced batch time of 103.9 minutes.

In conclusion, using optimal temperature trajectories shows great promise in terms of time savings associated with producing one batch of polymer product, compared to optimal isothermal operation.

I would like to express my sincerest gratitude to Cybernetica AS for giving me the opportunity to work with this project. I am especially thankful to Peter Singstad, for high quality supervision, and to Fredrik Gjertsen, for welcoming me in his office with the attitude that no problem is too small. I would also like to thank my NTNU supervisor Associate Professor Johannes Jäschke for his support during the project work.

# Contents

<b>Abstract</b>	<b>i</b>
<b>List of Figures</b>	<b>iv</b>
<b>List of Tables</b>	<b>v</b>
<b>List of Abbreviations</b>	<b>vi</b>
<b>List of Symbols</b>	<b>vii</b>
<b>1 Introduction</b>	<b>1</b>
<b>2 Theory</b>	<b>2</b>
2.1 Polymers and Polymerization . . . . .	2
2.1.1 Free-Radical Polymerization . . . . .	2
2.2 Semi-Batch Reactor Modeling . . . . .	4
2.2.1 Mass and Energy Balances . . . . .	5
2.2.2 Conversion . . . . .	6
2.3 Polymerization Modeling . . . . .	6
2.3.1 The Method of Moments . . . . .	6
2.3.2 Average Molecular Weights . . . . .	7
2.3.3 The Polydispersity Index . . . . .	8
2.3.4 Free-Volume Theory and Diffusion-Controlled Reactions . . . . .	8
2.4 Parameter Estimation . . . . .	8
2.5 Optimization Basics . . . . .	10
2.5.1 Sequential Quadratic Programming . . . . .	12
2.6 Model Predictive Control . . . . .	13
2.7 The Control Hierarchy . . . . .	16
<b>3 Process Description</b>	<b>18</b>
3.1 Reaction Kinetics . . . . .	19
<b>4 Modeling</b>	<b>21</b>
4.1 Assumptions . . . . .	21
4.2 Dynamic Model Equations . . . . .	22
4.2.1 Component and Moment Balances . . . . .	22
4.2.2 Energy Balances . . . . .	26
4.3 Model Structure and Choice of Model Variables . . . . .	26
4.4 Implementation and Numerical Solving of the Model . . . . .	28
4.5 Results and Discussion . . . . .	28
4.5.1 Effect of Temperature and Monomer to Initiator Ratio . . . . .	28
4.5.2 Effect of Pentane . . . . .	32
<b>5 Offline Parameter Estimation</b>	<b>35</b>
5.1 Results and Discussion . . . . .	35
<b>6 Optimization</b>	<b>39</b>
6.1 Plantwide Optimization of EPS Production . . . . .	39
6.2 Formulation of the Optimization Problem . . . . .	40

6.3	Solving the Optimization Problem . . . . .	42
6.4	Results and Discussion . . . . .	44
6.4.1	Pre-Optimization Simulation . . . . .	45
6.4.2	Optimization of Monomer to Initiator Ratio . . . . .	47
6.4.3	Optimization of Monomer to Initiator Ratio and Constant Temperature .	49
6.4.4	Optimization of Monomer to Initiator Ratio and Temperature Profile . .	52
6.4.5	Summary . . . . .	56
<b>7</b>	<b>Conclusion</b>	<b>58</b>
<b>A</b>	<b>Model Parameters</b>	<b>I</b>
<b>B</b>	<b>Optimization of Monomer to Initiator Ratio and Temperature Profile with High Cooling Water Temperature</b>	<b>II</b>

## List of Figures

2.1	Molecular weight distribution. . . . .	7
2.2	Block diagram of online parameter estimation. . . . .	10
2.3	The difference between global and local minima. . . . .	12
2.4	Illustration of communication between the MPC application and the plant [1]. . . . .	15
2.5	Illustration of the concept of input blocking. . . . .	16
2.6	The control hierarchy. . . . .	16
3.1	A semi-batch reactor for suspension polymerization of styrene. . . . .	18
3.2	Activation of a new growing polystyrene chain and the propagation process. . . . .	19
4.1	Number average molecular weight simulation results. . . . .	29
4.2	Weight average molecular weight simulation results. . . . .	29
4.3	Styrene conversion simulation results. . . . .	30
4.4	Initiator content simulation results. . . . .	30
4.5	Apparent initiator efficiency simulation results. . . . .	31
4.6	Apparent propagation rate constant simulation results. . . . .	31
4.7	Apparent termination by combination rate constant simulation results. . . . .	32
4.8	Apparent termination and propagation rate constants and initiator efficiency simulation results for different amounts of pentane added. . . . .	33
4.9	Number and weight average molecular weight simulation results for different amounts of pentane added. . . . .	33
4.10	Monomer conversion and initiator consumption simulation results for different amounts of pentane added. . . . .	34
5.1	Temperature profile and pentane addition for parameter estimation. . . . .	36
5.2	$\bar{M}_w$ measurements and model predictions before and after parameter estimation. . . . .	37
5.3	$\bar{M}_n$ measurements and model predictions before and after parameter estimation. . . . .	37
6.1	Diagram of plantwide optimization of an EPS polymerization plant. . . . .	40
6.2	Conversion as a function of time with (dashed line) and without (solid line) interpolation. . . . .	44
6.3	Surface plot of $\bar{M}_n$ as a function of isothermal temperature and monomer to initiator ratio. . . . .	45
6.4	Surface plot of batch time as a function of isothermal temperature and monomer to initiator ratio. . . . .	46
6.5	Number and weight average molecular weights for monomer to initiator ratio optimization at 113.5 °C. . . . .	47
6.6	Monomer conversion and initiator consumption for monomer to initiator ratio optimization at 113.5 °C. . . . .	48
6.7	Cooling demand and cooling capacity constraint for monomer to initiator ratio optimization at 113.5 °C. . . . .	49
6.8	Number and weight average molecular weights for monomer to initiator ratio and constant temperature optimization. . . . .	50
6.9	Monomer conversion and initiator consumption for monomer to initiator ratio and constant temperature optimization. . . . .	51
6.10	Cooling demand and cooling capacity constraint for monomer to initiator ratio and constant temperature optimization. . . . .	52
6.11	Number and weight average molecular weights for monomer to initiator ratio and temperature profile optimization. . . . .	53
6.12	Styrene conversion and initiator consumption for monomer to initiator ratio and temperature profile optimization. . . . .	54

6.13	Temperature profile and cooling demand for monomer to initiator ratio and temperature profile optimization. . . . .	55
6.14	Temperature profile and cooling demand for cooling water temperatures of 10 and 20 °C. . . . .	56
B.1	Number and weight average molecular weights for monomer to initiator ratio and temperature profile optimization. . . . .	II
B.2	Styrene conversion and initiator consumption for monomer to initiator ratio and temperature profile optimization. . . . .	II
B.3	Temperature profile and cooling demand for monomer to initiator ratio and temperature profile optimization. . . . .	III

## List of Tables

4.1	Solubility of styrene, polystyrene and pentane in water, and vice versa, at 20 °C.	21
6.1	Values of the parameters in the optimization problem. . . . .	42
6.2	Weights in the optimization of monomer to initiator ratio and reactor temperature trajectory. . . . .	52
6.3	Key numbers from the optimization results. . . . .	56
A.1	Values of the parameters used in the model. . . . .	I

## List of Abbreviations

---

<b>Abbreviation</b>	
CLD	Chain Length Distribution
CTA	Chain Transfer Agent
DCP	Dicumyl Peroxide
DRTO	Dynamic Real-Time Optimization
EKF	Extended Kalman Filter
EPS	Expandable Polystyrene
FMI	Functional Mock-up Interface
LP	Linear Program
MPC	Model Predictive Control
MWD	Molecular Weight Distribution
NLP	Nonlinear Program
NMPC	Nonlinear Model Predictive Control
OPC	Open platform communication
PDI	Polydispersity Index
PSSA	Pseudo-Steady State Assumption
SQP	Sequential Quadratic Programming
QP	Quadratic Program

---

## List of Symbols

Symbol	Description	Unit
$a$	Translational diffusion tuning parameter	—
$A$	Translational diffusion tuning parameter	—
$A_{cr}$	Gel effect critical frequency factor	—
$AH$	Diels-Alder adduct molecule	
$A_l$	Gel effect tuning parameter	—
$B$	Glass effect tuning parameter	—
$C$	Cage effect tuning parameter	—
$C5$	Pentane molecule	
$c_i$	Constraint number $i$	
$c_{p,i}$	Heat capacity of component $i$	J/kgK
$c_{p,v}$	Heat capacity of reactor vessel	J/kgK
$c_{p,R}$	Heat capacity of reactor content	J/kgK
$c_{p,tot}$	Total heat capacity	J/K
$dT_R$	Derivative of reactor temperature	K/s
$d_{u_k}$	Linear input weighting vector	
$d_{x_k}$	Linear state weighting vector	
$d_{\Delta u_k}$	Linear input change weighting vector	
$f$	Objective function/model function/initiator efficiency	
$f_{app}$	Apparent initiator efficiency	—
$g$	Measurement model function	
$h$	Output model function	
$H$	Enthalpy	J
$\hat{H}$	Enthalpy flow	W
$I$	Chemical initiator molecule	
$k$	Moment order/discrete time step	
$K$	Test parameter for gel effect	(kg/mol) <sup>0.5</sup>
$K_{cr}$	Critical parameter for gel effect	(kg/mol) <sup>0.5</sup>
$k_d$	Decomposition of initiator rate constant	1/s
$k_{dm}$	Thermal initiation rate constant	m <sup>6</sup> /mol <sup>2</sup> s
$k_e$	Example reaction rate constant	m <sup>3</sup> /s
$k_i$	Monomer addition to initiator radical rate constant	m <sup>3</sup> /mol · s
$K_k$	Gain matrix	
$k_p$	Propagation rate constant	m <sup>3</sup> /mol · s
$k_{p,app}$	Apparent propagation rate constant	m <sup>3</sup> /mol · s
$k_{tc}$	Termination by combination rate constant	m <sup>3</sup> /mol · s
$k_{tc,app}$	Apparent termination rate constant	m <sup>3</sup> /mol · s
$k_{tc,rd}$	Residual diffusion termination rate constant	m <sup>3</sup> /mol · s
$k_{tc,seg}$	Segmental diffusion-controlled termination rate constant	m <sup>3</sup> /mol · s
$k_{tc,trans}$	Translational diffusion-controlled termination rate constant	m <sup>3</sup> /mol · s
$k_{td}$	Termination by disproportionation rate constant	m <sup>3</sup> /mol · s
$k_{trd,max}$	Maximum value of residual diffusion contribution	m <sup>3</sup> /mol · s
$k_{trd,min}$	Minimum value of residual diffusion contribution	m <sup>3</sup> /mol · s
$k_{trM}$	Transfer to monomer rate constant	m <sup>3</sup> /mol · s

$k_{trT}$	Transfer to chain transfer agent rate constant	$\text{m}^3/\text{mol} \cdot \text{s}$
$K_Q$	Heat transfer coefficient	$\text{W}/\text{K}$
$k_1$	Diels-Alder reaction rate	$\text{m}^3/\text{mol} \cdot \text{s}$
$l$	Gel effect tuning parameter	—
$n$	Chain length	—
$N$	Prediction horizon	—
$\bar{n}$	Number average chain length	—
$n_i$	Total molar amount of component i	$\text{mol}$
$\hat{n}_i$	Molar flow rate of component i	$\text{mol}/\text{s}$
$n_{I, fed}$	Fed amount of initiator	$\text{mol}$
$\hat{n}_{in}$	Molar flow rate into reactor	$\text{mol}/\text{s}$
$n_{I,0}$	Initial number of moles of initiator	$\text{mol}$
$n_{I,0,max}$	Upper bound on initial number of moles of initiator	$\text{mol}$
$n_{I,0,min}$	Lower bound on initial number of moles of initiator	$\text{mol}$
$n_{P,n}$	Amount of polymer chains with length $n$	$\text{mol}$
$n_r$	Number of decision variables	—
$n_u$	Number of input variables	—
$n_x$	Number of states	—
$M$	Monomer molecule	
$m_c$	Mass of cooling water	$\text{kg}$
$\hat{m}_c$	Flow rate of cooling water	$\text{kg}/\text{s}$
$\bar{M}_n$	Number average molecular weight	$\text{kg}/\text{mol}$
$\bar{M}_{n,d}$	Desired number average molecular weight	$\text{kg}/\text{mol}$
$\bar{M}_{n,f}$	End product number average molecular weight	$\text{kg}/\text{mol}$
$m_R$	Mass of reactor content	$\text{kg}$
$m_v$	Mass of reactor vessel	$\text{kg}$
$M_{w,M}$	Molecular weight of monomer	$\text{kg}/\text{mol}$
$\bar{M}_w$	Weight average molecular weight	$\text{kg}/\text{mol}$
$PI$	Polydispersity index	—
$P_n$	Polymer chain of length $n$	
$q$	Quadratic setpoint deviation weight for $\bar{M}_n$	—
$Q$	Added heat	$\text{W}$
$Q_{amb}$	Heat transferred to surroundings	$\text{W}$
$Q_J$	Heat transferred to cooling jacket	$\text{W}$
$Q_{J,d}$	Cooling demand to keep desired temperature	$\text{W}$
$Q_{J,min}$	Cooling capacity constraint	$\text{W}$
$Q_k$	Quadratic state/output weighting matrix of time step $k$	
$r$	Combined vector of decision variables	
$R$	Gas constant	$\text{J}/\text{molK}$
$R_i$	Rate of consumption of component i	$\text{mol}/\text{m}^3\text{s}$
$R_k$	Quadratic input weighting matrix of time step $k$	
$R_n$	Radical chain of length $n$	
$R_p$	Propagation rate	$\text{mol}/\text{m}^3\text{s}$
$r_1$	Linear weights on constraint slack variables	
$r_2$	Quadratic weights on constraint slack variables	
$s_{dT_R}$	Quadratic change rate weight for temperature derivative	—
$S_k$	Quadratic input change rate weighting matrix of time step $k$	
$t$	Time	$\text{s}$

$T$	Transfer agent molecule	
$T_{amb}$	Ambient temperature	K
$t_f$	Batch time	min
$T_{feed}$	Feed temperature	K
$t_{f,max}$	Upper bound on batch time	s
$t_{f,min}$	Lower bound on batch time	s
$T_{g,i}$	Glass transition temperature of component $i$	K
$T_J$	Cooling jacket temperature	K
$T_{J,const}$	Constant cooling jacket temperature	K
$T_R$	Reactor temperature	K
$T_{R,max}$	Upper bound on reactor temperature	°C
$T_{R,min}$	Lower bound on reactor temperature	°C
$T_{R,ref}$	Reference reactor temperature	K
$u$	Input vector	
$(UA)_{amb}$	Overall heat transfer coefficient, heat loss	W/K
$(UA)_J$	Overall heat transfer coefficient, cooling jacket	W/K
$u^{high}$	Upper bounds on inputs	
$u^{low}$	Lower bounds on inputs	
$V$	Polymer phase volume	m <sup>3</sup>
$V_{f,i}$	Free volume of component $i$	—
$W_{ag}$	Agitation work	W
$W_s$	Shaft work	W
$x$	State vector	
$X$	Overall conversion	
$X_d$	Desired conversion	—
$x^{high}$	Upper bounds on states	
$X_{inst}$	Instantaneous conversion	—
$x^{low}$	Lower bounds in states	—
$x_{ref}$	State reference trajectory	
$x_0$	Initial state	
$x^*$	Local minimizer	
$y_m$	Plant measurements	
$\hat{y}_m$	Measurements predicted by measurement history	
$y_p$	Measurements predicted by model	
$z$	Output/controlled variable	
$\alpha_i$	Fractional free volume of component $i$	—
$\delta_c$	Segmental diffusion parameter	—
$\Delta H_R$	Reaction enthalpy	J/m <sup>3</sup> s
$\Delta t_{int}$	Integration time step	s
$\Delta dT_R$	Change of temperature derivative between two samples	K/s
$\Delta u^{high}$	Upper bounds on input change rate	
$\Delta u^{low}$	Lower bounds on input change rate	
$\Delta \tau$	Linear interpolation time step	s
$\epsilon$	Constraint slack variables	
$\eta$	Chosen parameters for offline estimation	
$\theta$	Parameter vector	
$\hat{\theta}$	Estimated parameter vector	
$\lambda_0$	Zeroth order moment, living chains	mol

$\lambda_1$	First order moment, living chains	mol
$\lambda_2$	Second order moment, living chains	mol
$\mu_k$	$k^{th}$ order moment	–
$\mu_0$	Zeroth order moment, dead chains	mol
$\mu_1$	First order moment, dead chains	mol
$\mu_2$	Second order moment, dead chains	mol
$\tau_I$	Initiator feed time constant	s
$\mathcal{E}$	Set of equality constraints	
$\mathcal{I}$	Set of inequality constraints	

---

# 1 Introduction

Synthetic polymers in the form of plastics have become a natural part of our everyday existence. One of the biggest commodity polymer products in the world is expandable polystyrene (EPS), which is the polymer of focus in this work. In 2014, the European demand for EPS was about 1.5 million tonnes. It is a thermoplastic product in the form of a solid foam with low density, high moisture resistance, high durability and excellent insulating properties. Because of these qualities, EPS is an ideal material for packaging of food and other goods, and for construction purposes [2].

Producers of EPS are today facing an ever-increasing competition and highly demanding markets where reliable and consistent earnings are issues. Because of the extent of the EPS production and the low product price, increasing plant capacity utilization is key for EPS manufacturers to increase profitability [3]. An efficient way to address the goal of maximum production is to lower the time associated with producing each batch of polymer product at the desired product quality, as well as ensuring that available resources are distributed according to optimal operation.

A possible approach to achieve better utilization of the plant is to use optimal control to steer the semi-batch reactor through the optimal conditions that give the desired product quality in the shortest possible polymerization time. There are two main reasons why such strategies are not extensively used in the polymer industry today. First of all, optimal control of batch reactors and semi-batch reactors requires accurate dynamic models. Such models are time consuming and costly to develop, as they must be tailored for the specific process. In contrast, process industries using continuous processes, where stationary process models are sufficient for optimal control, have applied such control strategies for a long time [4]. Secondly, efficient numerical solvers capable of solving complex nonlinear optimization problems with large numbers of variables involved have not been developed before recent times. As a consequence, the available solution methods have limited the research and applications of optimal control strategies in the way that the process models used have been rigorously simplified, resulting in inaccurate optimal conditions [5]. These days, the computational power required to solve complex chemical engineering problems are facilitated by personal computers found at every office work-place, meaning that time is ripe to continue the work into optimal control of batch and semi-batch processes [6].

The scope of this work is to develop a simple process model for a semi-batch reactor for production of EPS, including parameter estimation to fit the model to real plant data. Further, this model is used to perform offline optimization of the batch duration according to constraints on the cooling capacity of the reactor. The degrees of freedom used in the optimization routine is the temperature of the batch reactor and the initial reactor recipe. This work could be used as a pre-stage of an implementation of dynamic real-time optimization and model predictive control.

## 2 Theory

### 2.1 Polymers and Polymerization

Polymers are defined as materials of very high molecular weight. Such materials have numerous applications in our modern society, although they have been around for a long time. Natural materials like rubber, silk, wool and cotton are polymers. Today, polymers are found in clothing, food packaging, home furnishing, paint products, toys, building insulation, information technology products and more [7].

Polymers are made up of smaller building blocks of chemical compounds called monomers, and they are usually consisting of repetitive structural units. They can hold hundreds, thousands or even tens of thousands of monomers [8]. For example, the polymer *polyethylene* is made of the repetitive units  $[-\text{CH}_2-\text{CH}_2-]_n$ , and the monomers chained together are ethylene molecules, as the name indicates.  $n$  is the number of monomer units in the polymer, or what is also referred to as the *chain length* [7]. Homopolymers are polymers made up of one single kind of monomer, while copolymers have two or more monomer unit types. Polymers can consist of straight chains, branched chains or chain networks [8].

Polymerization is the process where monomers combine to become polymers. There are several different kinds of kinetic mechanisms resulting in polymerization. They can be distinguished into *step-growth polymerizations* (polycondensations) and *chain polymerizations*. Step-growth polymerization is usually a result of a chemical reaction between two functional groups. In chain polymerization, monomers are added to the chain one by one. This type of polymerization can proceed via free-radical, anionic, cationic, group-transfer and coordination mechanisms [8].

Also the process characteristics for which the polymerization process is carried out can vary. In *bulk polymerization*, the monomer makes up the bulk of the reactor, containing only small amounts of catalyst and additives. The reaction mixture of a bulk polymerization has a tendency of reaching high viscosity levels during the reaction. To avoid problems related to high viscosity, a solvent is sometimes added, giving a *solution polymerization process*. Both of these polymerization processes contain one single phase, while *precipitation polymerization* has both a liquid phase and a solid phase, as the polymer is insoluble in its monomer. Other two-phase polymerization processes are the *suspension polymerization*, where the polymerization proceeds in small beads in a continuous phase, and *emulsion polymerization*, where the reaction takes place in micelles in a water phase [8].

Classification of polymers is not uniform, and can be done according to many different criteria [8]:

- Chemical nature of polymer
- Molecular structure of polymer
- Polymer chain growth mechanism
- Type of polymerization process

#### 2.1.1 Free-Radical Polymerization

Free-radical polymerization is driven by the addition of a monomer molecule to a radical active center. A free radical is an unpaired electron, which gives rise to highly reactive chemical

compounds.

All free-radical polymerization processes consists of the three basic reaction types: initiation, propagation and termination. Initiation reactions form radicals continuously during the process, and are responsible for activating new polymer chains. Growth of the polymer chains is a result of the propagation reaction, while the generation of inactive polymer chains is caused by termination of active chains. In addition, numerous different chain transfer reactions can occur, where a free radical is transferred from one molecule to another [8].

Initiation is caused by a chemical compound with the ability to form radical molecules. Chemical initiators are normally organic peroxides, with a covalent oxygen bond separating two organic groups. Decomposition of this bond results in two radical molecules, according to the chemical reaction 2.1. Here,  $f$  is the initiator efficiency, which is a number between 0 and 1, and  $k_d$  is the rate constant of the decomposition reaction.



The simplest form of peroxide initiators is the mono-functional initiator with one peroxide group. Initiators that have two peroxide groups are called bi-functional initiators [9]. These are more complicated to handle in modeling as growing chains can contain an undecomposed peroxide group that can decompose at a later stage to form new radicals.

The primary radicals  $I \cdot$  generated in the decomposition reaction combine with a monomer molecule  $M$  to give a radical polymer chain of length 1 ( $R_1$ ), according to:



The rate of monomer addition to the initiator radical is determined by the rate constant  $k_i$ .

Most of the active chain seeds produced in the initiation step will undergo propagation, at a rate given by  $k_p$ . This reaction occurs simultaneously to radical chains of all sizes.



There are several ways that a radical chain  $R$  can be deactivated to produce an inactive polymer chain  $P$ . In *termination by combination*, shown in 2.4, two radical chains meet and form a covalent carbon-carbon bond from their free radicals. This produces a dead chain with chain length equal to the sum of the lengths of the two chains.



Another termination type is the *termination by disproportionation*. Here, two radical chains meet, and one of the chains transfers its radical to the other chain, giving two dead polymer chains.



Similarly to the termination reactions, chain transfer is also a way of ending a growing polymer chain. Chain transfer reactions occur between active radical chains and a chain transfer agent  $T$ ,

which could be many of the different components in the reaction mixture, for instance monomer molecules. If impurities are present in the reaction mixture, these can act as unintended transfer agents. In some cases, this effect is exploited to control chain length of the produced polymer, and so-called chain transfer agents (CTA) are added.



### Diffusion-Controlled Reactions:

As the polymer chains grow, the viscosity of the polymer phase increases and the volume of the reactive mass is reduced. Consequently, some of the reactions 2.1-2.6 could at some point during the process become diffusion-controlled.

The most important diffusion limiting effect influences the rate of termination, and is known as the *gel effect* or *Trommsdorff-Norrish effect*. When polymer chains grow and the polymer phase becomes viscous, the polymer chains will be hindered in diffusing freely in the polymer phase. This results in a drop in the chain termination rate, giving a broader molecular weight distribution [8]. Hence, the final product properties are altered. Severe gel effect could even pose a safety risk, as it could lead to a dominant propagation reaction, which make up most of the heat generation in the reaction system. Such conditions could cause the heat generation from the reaction to exceed the heat removal provided by the cooling system. Consequently, the temperature inside the reactor will increase, resulting in a boost of the reaction rates and eventually, loss of control of the polymerization process. This phenomenon is named *thermal runaway* [10].

Diffusional limitations affecting the efficiency of the chemical initiator is commonly known as the *cage effect*. At high monomer conversions, the number of active initiator radicals contributing to the polymerization process will decrease. This effect is mainly caused by polymer chains surrounding the active radicals, constituting a “cage” and hindering the radicals from moving freely. Inside such a cage, an active initiator radical is likely to self-terminate or react with other neighboring molecules instead of initiating a new chain [11].

The equivalent effect for the propagation reaction is called the *glass effect*. As the name suggests, this effect is highly influenced by the glass transition temperature of the polymer, which is the lower temperature limit inducing a structural change in the polymer; from being soft and flexible (rubbery) to becoming hard and brittle [12]. Therefore, the glass effect increases with reduced temperature. If the polymerization temperature is sufficiently close to the glass transition temperature, the probability of collisions between active polymer chains and free monomer molecules could fall drastically due to reduced mobility of the monomer. As a result, the propagation rate will diminish [8].

## 2.2 Semi-Batch Reactor Modeling

The semi-batch reactor possesses characteristics of both batch types and continuous types of processes. In a batch reactor, the reactants are loaded before the reactions are initiated. After the reactions have taken place, the products are removed. This is in contrast to the continuous-type process, where reactants are fed continuously and product is drained off while the reaction is ongoing. In a semi-batch process, some parts of the process are batch-type and some parts are continuous. Often, some reactants are loaded before initiation, and others are added through a feed stream during parts of the batch time [13].

### 2.2.1 Mass and Energy Balances

The most important part of modeling a semi-batch reactor is to keep balances of component mass and energy:

$$\text{Component balance: } \frac{dn_i}{dt} = R_i V + \hat{n}_i \quad (2.7a)$$

$$\text{Energy balance: } \frac{dH}{dt} = \hat{H} + Q + W_s - \Delta H_R R_i V \quad (2.7b)$$

In this formulation,  $n_i$  is the present amount of component  $i$ ,  $R_i$  is reaction rate and  $\hat{n}_i$  the molar feed flow. Moreover,  $H$  is the total enthalpy,  $\hat{H}$  is the enthalpy of the feed stream,  $Q$  is added heat,  $W_s$  is added shaft work,  $\Delta H_R$  is reaction enthalpy and  $V$  is the reaction mixture volume. The subscript  $i$  denotes an arbitrary component in the system. Since components are removed and generated by reactions within the reaction mixture, it is convenient to choose component balances on molar form.

The reaction rate term gives the frequency of formation and removal of a component in the reaction volume. For an example reaction  $A \xrightarrow{k_e} B$ , the reaction rates of the two components A and B are given by:

$$R_A = -k_e[A] \quad (2.8a)$$

$$R_B = k_e[A] \quad (2.8b)$$

, where  $k_e$  is the rate constant of the reaction, and  $[A]$  is the concentration of component A.

The energy balance in Equation 2.7b is often transformed from an enthalpy balance to a temperature equation, mainly because temperature is an easily measured and highly relatable property. Transforming the energy balance to temperature form yields:

$$\frac{d}{dt} \left( \underbrace{m_v c_{p,v} T_R}_{\text{Vessel}} + \underbrace{m_R c_{p,R} T_R}_{\text{Content}} \right) = \hat{H} + Q_J + Q_{amb} + W_s - \Delta H_R R_i V \quad (2.9)$$

$$\implies \frac{dT_R}{dt} = \frac{\hat{H} + Q_J + Q_{amb} + W_s - \Delta H_R R_i V}{m_v c_{p,v} + m_R c_{p,R}} \quad (2.10)$$

Here,  $m_v$  and  $c_{p,v}$  are the mass and heat capacity of the reactor vessel, respectively. The corresponding variables for the reactor content has the symbols  $m_R$  and  $c_{p,R}$ , while  $T_R$  is the temperature of the reactor content. The added heat  $Q$  has here been divided into the contributions from the surroundings  $Q_{amb}$  and the cooling or heating system  $Q_J$ .

If the reactor temperature is controlled to a desired value or trajectory, it is sometimes useful to know the magnitude of the heat transfer required by the cooling or heating system. This magnitude can be referred to as *cooling* or *heating demand*, and is calculated by reformulating the temperature equation. The result is the following:

$$Q_{J,d} = c_{p,tot} \frac{dT_{R,ref}}{dt} + \Delta H_R R_i V - \hat{H} - Q_{amb} - W_s \quad (2.11)$$

Here,  $\frac{dT_{R,ref}}{dt}$  is the desired rate of temperature change in the reactor and  $c_{p,tot}$  is the total heat capacity. If isothermal operation is desired, this derivative is set to zero.

### 2.2.2 Conversion

Conversion is the ratio between the amount of a basis component that has reacted and the fed amount of the same reactant, and simply represents the proportion of available reactant that has been converted to product [14]. For semi-batch reactors, two types of conversion can be calculated; the overall conversion and the instantaneous conversion. These conversion formulations are shown in Equation 2.12, and they apply to a semi-batch reactor operated between time  $t = 0$  and  $t = t_f$  [15].  $n(t)$  represents the amount of reactant present in the system at time  $t$ , and  $\hat{n}_{in}$  is the flow of reactant into the system.

$$\text{Overall conversion:} \quad X = \frac{n(t=0) + \int_0^t \hat{n}_{in}(\tau) d\tau - n(t)}{n(t=0) + \int_0^{t_f} \hat{n}_{in}(\tau) d\tau} \quad (2.12a)$$

$$\text{Instantaneous conversion:} \quad X_{inst} = \frac{n(t=0) + \int_0^t \hat{n}_{in}(\tau) d\tau - n(t)}{\int_0^t \hat{n}_{in}(\tau) d\tau} \quad (2.12b)$$

## 2.3 Polymerization Modeling

Because of the many involved reactions and the stochastic features of growing polymer chains, models of free-radical polymerization are potentially complex. Therefore, simplification methods involving moment balances and average molecular weights are frequently applied. In addition, diffusional limiting effects like the ones discussed in Section 2.1.1 play an important role, and must be included in the model accordingly.

### 2.3.1 The Method of Moments

A polymer product will consist of polymer chains of diverse lengths. The most accurate method to describe the product quality is therefore to use a molecular weight distribution (MWD) or chain length distribution (CLD). Controlling such distributions for the end product is useful, since the end-use properties of the product is highly dependent of its MWD. However, keeping population balances of polymer chains of different length results in a complicated model with a large number of states.

Alternatively, one could restore the most important characteristics of the MWD or CLD by using the method of moments, which is a statistical approach. For simplicity, an MWD is used further in this section to illustrate the value of moment balances.

The  $k^{th}$  order moment is given by:

$$\mu_k = \sum_{n=1}^{\infty} n^k \cdot n_{P,n} \quad (2.13)$$

, where  $n_{P,n}$  is the number of moles of polymer chains with length  $n$ .

The zeroth order moment gives the total area under the distribution curve, which for the MWD is the total amount of polymer chains. Furthermore, the first order moment gives for the MWD the amount of monomer molecules tied into polymer chains. The width of the distribution is reflected in the second order moment, meaning that a high value of the second order moment

is related to a heterogeneous mixture of chain lengths. Higher order moments are calculated in the same manner, although they are usually not required to reproduce the distribution characteristics [16].

In a free-radical polymerization, the different moment balances are applied on both living radical chains and terminated dead chains. The moments are tracked dynamically through the batch process by moment balances.

### 2.3.2 Average Molecular Weights

The moments explained in Section 2.3.1 are used to calculate two important average molecular weights, namely the number average molecular weight and the weight average molecular weight. The number average molecular weight is the ordinary arithmetic mean with the total polymer mass divided on the number of chains. Using moments, it is calculated as follows:

$$\bar{M}_n = \frac{\lambda_1 + \mu_1}{\lambda_0 + \mu_0} M_{w,M} \quad (2.14)$$

, where  $\bar{M}_n$  is the number average molecular weight.  $\lambda_k$  represents the  $k^{th}$  order moment of living chains and  $\mu_k$  are the corresponding dead chain moments.  $M_{w,M}$  is here the molecular weight of the monomer. If the polymer is a copolymer, the monomer molecular weight is replaced by the weighted average of the molecular weights of the involved monomers. The fraction part of this equation gives the number average chain length, which is sometimes used instead of number average molecular weight.

The weight average molecular weight calculation takes into account that long chains contain a larger portion of the total polymer mass. If one chooses a random chained monomer molecule, the chain it belongs to will on average have a weight equal to the weight average molecular weight. It is often referred to as  $\bar{M}_w$ , and is calculated as the fraction between the sum of second order moments and the sum of first order moments multiplied by the molar mass of the monomer.

$$\bar{M}_w = \frac{\lambda_2 + \mu_2}{\lambda_1 + \mu_1} M_{w,M} \quad (2.15)$$

The sketch shown in Figure 2.1 illustrates the principle of the relation of the number and weight average molecular weights to the MWD.

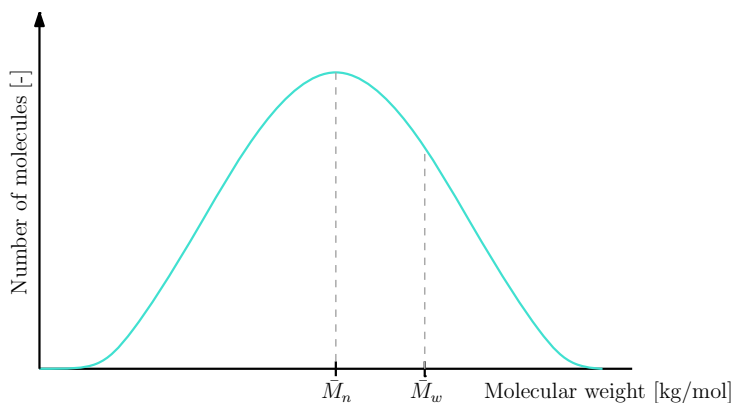


**Figure 2.1:** Molecular weight distribution.

### 2.3.3 The Polydispersity Index

The *polydispersity index*, also known as the *heterogeneity ratio* or *nonuniformity coefficient*, gives a measure on the width of the MWD. A large polydispersity index implies that the polymer product consists of chains of unequal length, whereas a polydispersity index equal to 1 means that all polymer chains are equally long. It is defined as the ratio between the weight average molecular weight and the number average molecular weight [17].

$$PI = \frac{\bar{M}_w}{\bar{M}_n} \quad (2.16)$$

### 2.3.4 Free-Volume Theory and Diffusion-Controlled Reactions

There exists many methods for modeling the diffusional limitations on the initiation, propagation and termination reactions mentioned in Section 2.1. Several varieties of comprehensive modeling methods that cover all three effects are based on *free-volume theory*.

Free-volume theory relates the diffusional limitations of polymer chains, initiator radicals and monomer molecules to the free volume surrounding these components. The free volume could be explained as the empty space between the molecules in the liquid phase. The free volume between molecules are divided in two parts: the *hole* free volume, which is the portion of the free volume which is continuously redistributed by thermal fluctuations, and the remaining *interstitial* free volume [18]. Diffusion processes in the liquid is, according to this theory, related to the hole free volume. When the polymer chains grow, chains start to overlap, and the polymer phase volume decreases, meaning that the elbowroom of the molecules is reduced, and the reactions in the polymer phase become diffusion-controlled. Additions of low viscosity additives will increase the free volume available for diffusion.

A detailed model of the cage, glass and gel effects based on free-volume theory is shown in Section 4.2.

## 2.4 Parameter Estimation

Parameter estimation is an important stage in the process of modeling a new plant. For first principle models, like the one developed in this work, the parameters obtained from literature, experiments or calculations may be uncertain. Parameter estimation is also a crucial part of developing data-driven models, where the parameters are completely unknown. In both cases, the objective is to estimate the parameters that best describe the real plant behavior, which is defined by measurements from the plant [19].

There are two main parameter estimation approaches; offline and online parameter estimation. Offline parameter estimation is used to adjust parameters that are time-invariant but uncertain. There are several offline parameter estimation methods in use. A simple and fairly common approach is solving a least squares optimization problem, where the quadratic difference between plant measurements and model predicted measurements is minimized [20]. The formulation of

such an optimization problem is shown in Equation 2.17.

$$\min_{\eta} \sum_{k=1}^N (y_{p,k}(x_k, u_k, \theta) - y_{m,k})^2 \quad (2.17a)$$

$$\text{s.t } x_{k+1} = f(x_k, u_k, \theta) \quad (2.17b)$$

$$y_{p,k} = g(x_k, u_k, \theta) \quad (2.17c)$$

$$\eta \subseteq \theta \quad (2.17d)$$

The solution to this problem is the chosen estimated parameters  $\eta$  which minimizes the squared difference between the predicted measurements  $y_{p,k}$  and the measurements from the plant  $y_{m,k}$ . Moreover, the formulation is in discrete time, meaning that the subscript  $k$  represents a point in time. The decision variables  $\eta$  must be chosen as a subset of the entire collection of parameters  $\theta$ . This minimization problem is subject to a range of discrete time constraints, which here implies that the model must be satisfied for the solution of  $\eta$ .

The optimization problem 2.17 is a nonlinear program because of the nonlinearities in the model constraints given by Equations 2.17b and 2.17c. A common method of solving such problems is the Sequential Quadratic Programming algorithm. These optimization related terms will be further explained in Section 2.5.

Online parameter estimation is used in cases where the parameters are uncertain and weakly varying. The model parameters are adjusted according to the real-time measurements from the plant. This allows for an improved match between the plant and the model, which facilitates for higher performance of model based control and optimization [4]. Online parameter estimation is often combined with estimation of the states. State estimates are useful in cases where the states are not measurable, or the measurements are unavailable, erroneous or noisy [21]. For instance, issues related to availability of credible measurements of the most important variables are predominant in polymer production processes. State estimates are in this case central to provide sufficient insight in order to apply optimal control. The block diagram 2.2 shows how the process model is updated online with state and parameter estimations, calculated from the model deviation from the plant measurements.

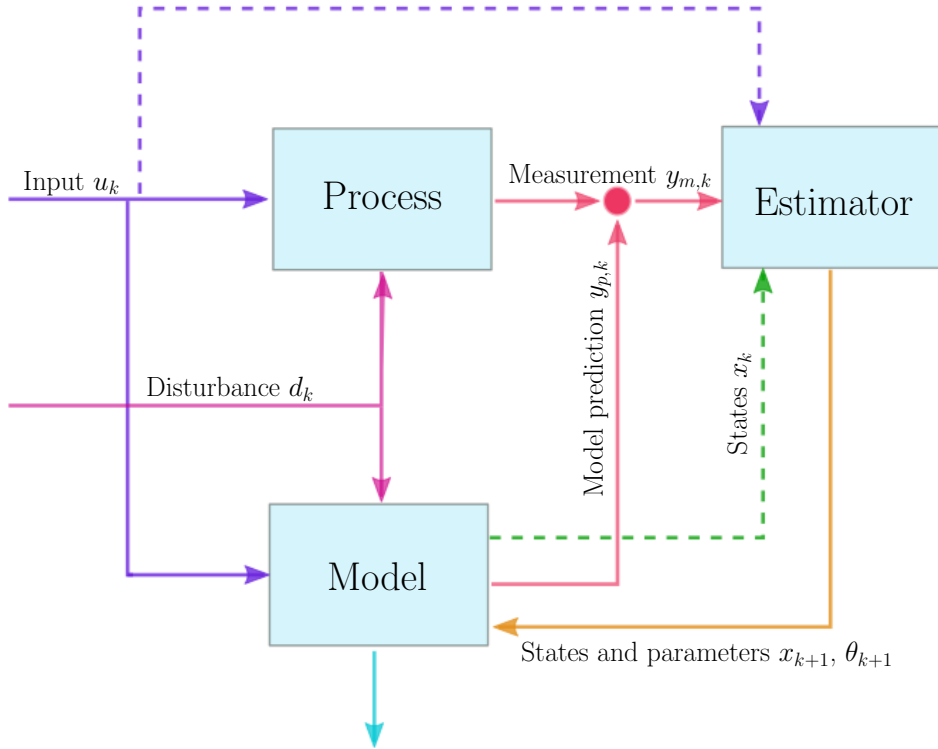


**Figure 2.2:** Block diagram of online parameter estimation.

Online parameter estimation methods are often based on recursive algorithms, which are efficient in the sense of memory usage, since new parameter estimates are based on the measurement history and previous parameter estimates [22]. A general formulation of a recursive estimation method can be formulated as follows:

$$\hat{\theta}_k = \hat{\theta}_{k-1} + K_k(y_{m,k} - \hat{y}_{m,k}) \quad (2.18)$$

$\hat{\theta}_k$  is the vector of estimated parameters at time step  $k$ , and the gain matrix  $K_k$  determines how much the deviation from the plant measurements will affect the updated parameters. The predicted measurements  $\hat{y}_{m,k}$  are functions of the observations up until time  $k - 1$ .

The most common recursive algorithm for state and parameter estimation is based on the Kalman Filter. The main idea of the Kalman Filter, proposed by Rudolf E. Kálmán in the late 1950s, was estimation of states [23]. The basic formulation of the Kalman Filter is derived for linear models, and the Extended Kalman Filter (EKF) algorithm contains an extension to nonlinear systems [4]. To include parameter estimation in these algorithms, the state vector is replaced by an augmented state vector which contains both states and parameters, and the result is the Augmented Kalman Filter.

## 2.5 Optimization Basics

In the general optimization problem, as formulated in 2.19, the aim is to minimize a scalar function referred to as the *objective function* ( $f$ ). The objective function is a function of one

or more decision variables ( $r$ ). The solution of the optimization problem is a set of values for these decision variables that fulfill the minimization aim. The choice of such decision variables is often limited by constraints  $c_i$ , meaning that only some solutions to the optimization problem are valid. Constraints are normally divided into two types, *equality constraints* and *inequality constraints*. The indexes belonging to the two types of constraints are held in the two index sets  $\mathcal{E}$  and  $\mathcal{I}$  for equality constraints and inequality constraints, respectively.

$$\min_{r \in \mathbb{R}^{n_r}} f(r) \tag{2.19a}$$

$$\text{subject to } c_i(r) = 0, i \in \mathcal{E} \tag{2.19b}$$

$$c_i(r) \geq 0, i \in \mathcal{I} \tag{2.19c}$$

The defined general optimization problem is a *nonlinear program* (NLP), because both the objective function and the constraints could be nonlinear. A quadratic programming (QP) problem is a special case of the general optimization problem where the objective function is quadratic and the constraints are linear. If an optimization problem has both linear objective function and linear constraints, it is called a linear programming (LP) problem.

*Global* and *local* solutions to optimization problems are normally distinguished between. An objective function could have several local minima, where the requirements of optimality are fulfilled. For unconstrained problems the main requirement of optimality is stated in the theorem below by Nocedal and Wright [24]. It says that the gradient of the objective function with respect to the decision variables is zero in a local minimum point.

**Theorem 1** (First-Order Necessary Conditions). *If  $x^*$  is a local minimizer and  $f$  is continuously differentiable in an open neighborhood of  $x^*$ , then  $\nabla f(x^*) = 0$ .*

Hence, for the unconstrained case, the zero gradient requirement could hold at several points, where one of them would be the global minimum. This difference is illustrated in Figure 2.3.

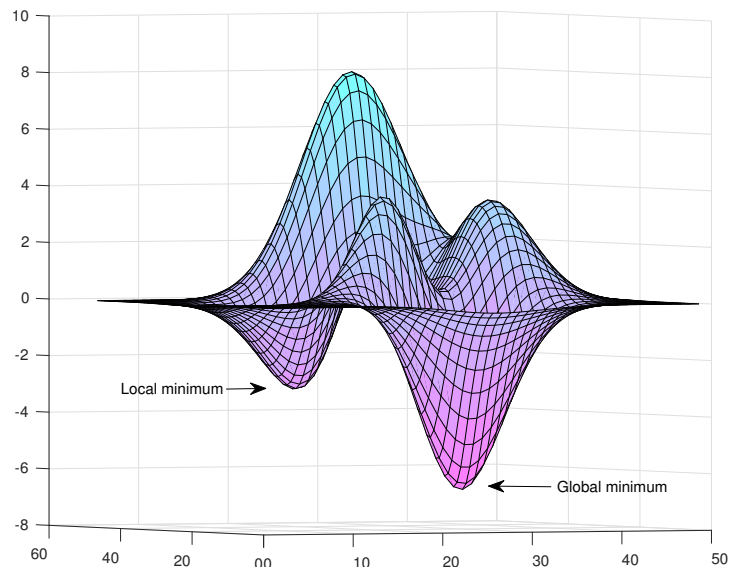


**Figure 2.3:** The difference between global and local minima.

The problem of finding the global minimum, or knowing that the found solution is the global minimum, is a major challenge for many optimization algorithms. For an important subclass of optimization problems called *convex problems*, this challenge is avoided. This is because the fact that an arbitrary local solution of a convex optimization problem is guaranteed to be a global solution, as stated in Theorem 2 from Nocedal and Wright [24].

**Theorem 2.** *When  $f$  is convex, any local minimizer  $x^*$  is a global minimizer of  $f$ . If in addition  $f$  is differentiable, then any stationary point  $x^*$  is a global minimizer of  $f$ .*

### 2.5.1 Sequential Quadratic Programming

Sequential Quadratic Programming (SQP) is known as one of the most successful methods for solving NLP problems. It uses an iterative procedure where a QP subproblem of the main NLP is solved at each iteration. Each subproblem is solved with the use of an appropriate method, such as the *active set method* or the *interior-point method*. The subproblems are constructed in a way that ensures convergence to a local minimum of the NLP as the number of iterations approach infinity [24].

A disadvantage of many optimization algorithms is that a feasible starting point has to be provided to initiate the algorithm. The SQP method avoids this problem by penalizing violation of constraints as a part of the objective function, instead of forcing every iteration point to be feasible. If the constraint violation is sufficiently weighted, convergence to a feasible solution is ensured.

More information on the SQP method, including a full derivation, can be found in Nocedal and Wright [24].

## 2.6 Model Predictive Control

Model predictive control (MPC) is a control concept that merges dynamic optimization and feedback control. Dynamic optimization is optimization on dynamic models, hence it seeks to minimize costs or maximize benefits over a period of time. As a result of this, the solution of dynamic optimization problems are functions of time. Sometimes, dynamic optimization is referred to as *optimal control*, as this area of optimization is often used to predict future optimal control actions to reach a specific goal [25]. Dynamic models can be given in both discrete and continuous time, and each of these two cases require a different approach to solving the problem [26].

In MPC, a discrete dynamic optimization problem over a prediction horizon  $N$  is solved at every time instant. The prediction horizon is the number of time steps into the future for which the optimal input usage  $u$  and the resulting predicted states  $x$  are calculated. The general form of the optimization problem is shown in Equation 2.20.

$$\begin{aligned} \min_{r \in \mathbb{R}^{n_r}} \quad & f(r) = \sum_{k=0}^{N-1} \frac{1}{2} (x_{k+1} - x_{k+1}^{ref})^T Q_{k+1} (x_{k+1} - x_{k+1}^{ref}) + d_{x_{k+1}} (x_{k+1} - x_{k+1}^{ref}) + \frac{1}{2} u_k^T R_k u_k \\ & + d_{u_k} u_k + \frac{1}{2} \Delta u_k^T S_k \Delta u_k + d_{\Delta u_k} \Delta u_k + r_1^T \epsilon + \frac{1}{2} \epsilon^T \text{diag}(r_2) \epsilon \quad (2.20a) \\ \text{subject to} \quad & x_{k+1} = f(x_k, u_k) \quad t = 0, \dots, N-1 \quad (2.20b) \\ & z_k = h(x_k, u_k) \quad t = 0, \dots, N-1 \quad (2.20c) \\ & x_0, u_{-1} = \text{given} \quad (2.20d) \\ & x^{low} - \epsilon \leq x_k \leq x^{high} + \epsilon \quad t = 1, \dots, N \quad (2.20e) \\ & u^{low} \leq u_k \leq u^{high} \quad t = 0, \dots, N-1 \quad (2.20f) \\ & \Delta u^{low} \leq \Delta u_k \leq \Delta u^{high} \quad t = 0, \dots, N-1 \quad (2.20g) \\ & Q_k \succeq 0 \quad t = 1, \dots, N \quad (2.20h) \\ & R_k \succeq 0 \quad t = 0, \dots, N-1 \quad (2.20i) \\ & S_k \succeq 0 \quad t = 0, \dots, N-1 \quad (2.20j) \end{aligned}$$

The objective function 2.20a penalizes state deviation from a desired reference  $x_{k+1}^{ref}$ , as well as usage of the inputs, the input change rate  $\Delta u_k$  and the slack variables  $\epsilon$  that represents deviation from hard state constraints. It contains both quadratic and linear weights for each of the penalized variables. For linear weighting, the value of the weighted term increases instantly when the variable moves away from the reference value. Quadratic weights give a low value gradient in the interval around the reference value, and will therefore provide a smaller penalty for a small deviation from the reference. On the other hand, a large deviation from optimality is penalized more, compared to linear weighting.

The quadratic state weighting matrix  $Q_{k+1}$  and the linear state weighting vector  $d_{x_{k+1}}$  gives an opportunity of giving the individual states different importance in the solution. It could for instance be crucial that some states quickly converge to the reference, while others might have less priority. The state weighting also provides an opportunity of weighting the importance of state convergence against the importance of the other variables in the objective function, such as input variables. For cheap and accessible inputs, the input weights could be chosen small

compared to the state weights. As for the states, the quadratic weights  $R_k$  and linear weights  $d_{u_k}$  for inputs could also be used for internal tuning of input priority.

The input change rate is penalized to minimize wear and tear on equipment, for instance valves. Increasing the weights on these variables also contribute to less aggressive control moves, which is a highly desired property of control behavior in large and complex industrial plants.

The slack variables  $\epsilon$  are added to the state constraints and penalized in the objective function to ensure that the solution of the optimization problem is feasible at all times [1]. Infeasibility of the optimization problem could namely occur if a disturbance pushes the states outside their bounds between two sampling instants. Larger weights  $r_1$  and  $diag(r_2)$  on the slack variables will result in a large cost, increasing the incentive to bring the states within the state bounds.

The only feasible solutions of  $x$  and  $u$  are those that follow the model constraints given by Equation 2.20b. In many cases, it is desired to control the output variables  $z$  rather than the states. In that case, the state variables in the objective function are simply replaced by output variables  $z_{k+1}$ , which are defined by the constraints 2.20c.

The constraints 2.20e and 2.20f act as upper and lower limits of the states and input variables. For the states, these could for instance be temperature or pressure limits. Similarly, for the inputs, these limits are often physical constraints such as the maximum and the minimum opening of a valve. The following constraints, given in Equation 2.20g, are upper and lower limits on the change of input usage from one time step to another. These constraints are also often related to physical limits such as the maximum opening or closing rate of a valve. The last equations in the formulation (Equations 2.20h-2.20i) imply that the weighting matrices  $Q_k$ ,  $R_k$  and  $S_k$  should be positive semidefinite.

Nonlinear model predictive control (NMPC) is a special case of MPC where the model function  $f$  is a nonlinear function. Solving the dynamic optimization problem for an NMPC case requires use of a nonlinear solver such as SQP.

By applying only the first input of the optimal input trajectory to the process, and using the current (measured or estimated) state as the initial condition, feedback is included. This way, any deviation from desired behavior of the states is noticed and the solution input trajectory of the next iteration will adjust to counteract this deviation. The relation between the MPC prediction calculation and the real plant is shown in Figure 2.4.

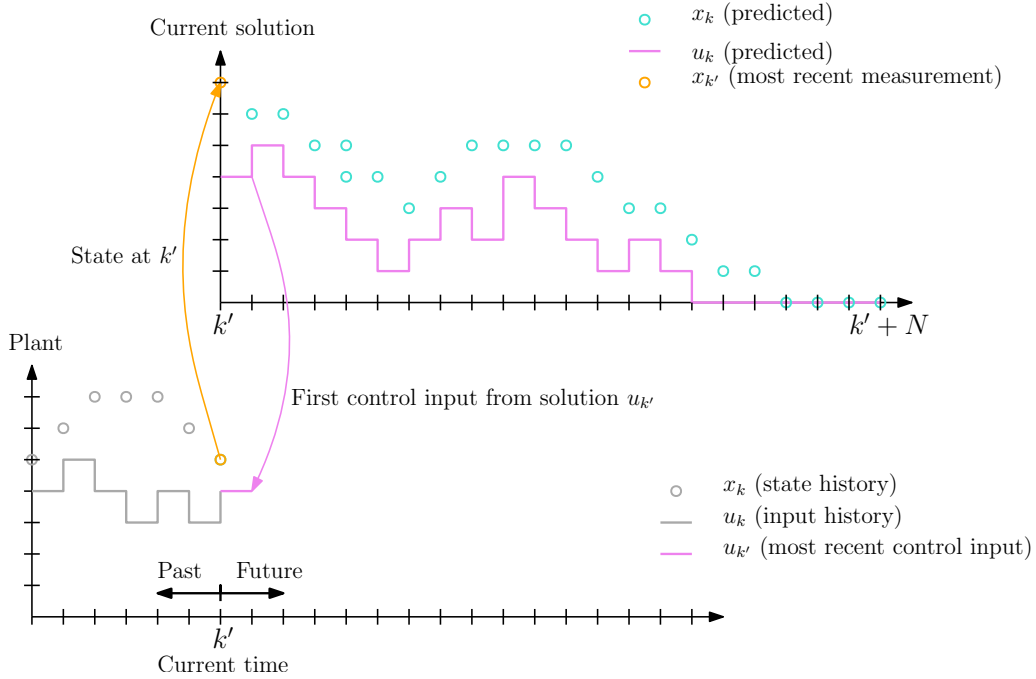


**Figure 2.4:** Illustration of communication between the MPC application and the plant [1].

The required computational effort associated with solving the dynamic optimization problem 2.20 is highly dependent on the number of decision variables, which is given by:

$$n_r = N(n_x + n_u) \tag{2.21}$$

, where  $n_x$  and  $n_u$  is the number of state and input variables, respectively.

An efficient way of reducing the number of decision variables, and thus the computation time, is to use *control input blocking*. In input blocking, the manipulated variables are forced to take constant values over intervals spanning one or more time steps. Usually, the input variables are allowed to move frequently in the beginning of the prediction horizon, with increasing block lengths towards the end, as the states tend to settle to a steady value here. The concept of input blocking is illustrated in Figure 2.5. Practice has shown that input blocking works well in terms of reducing computational effort with little consequences in control quality [1].

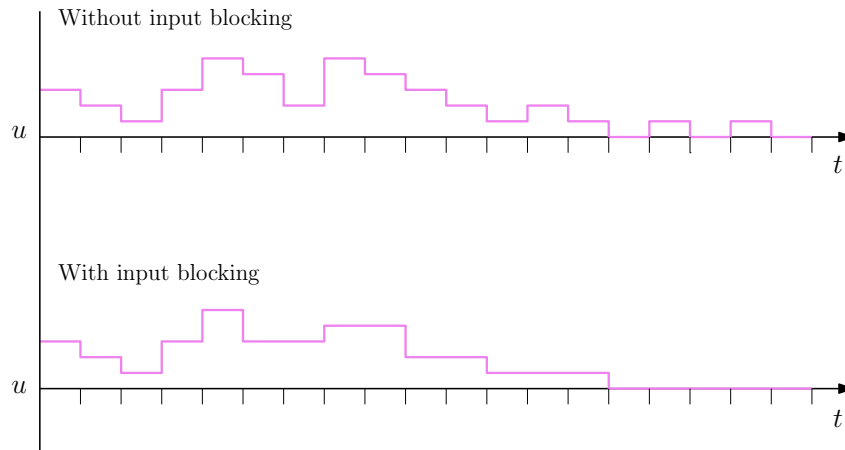


**Figure 2.5:** Illustration of the concept of input blocking.

## 2.7 The Control Hierarchy

A convenient way of structuring a control system is using layering in a control hierarchy based on differences in the frequency of the performed tasks [1]. Such a control hierarchy is illustrated in Figure 2.6.

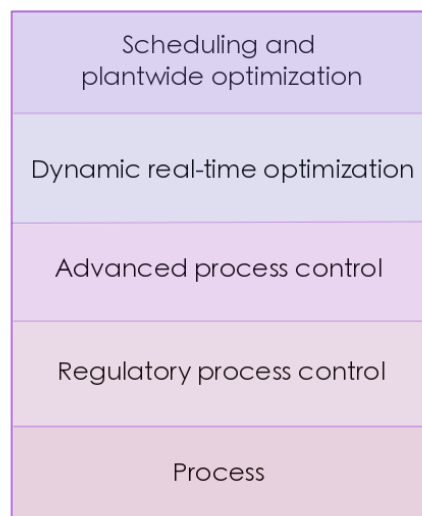


**Figure 2.6:** The control hierarchy.

On the top of the hierarchy, tasks that belong to the time scale of weeks and months are placed. This layer handles scheduling, evaluations of the product market demand and procurement of raw material. It could also contain evaluations and optimization calculations on distribution of available resources and production plans on different products. Based on these calculations and evaluations, constraints and information on desired plant throughput are passed down to the next layers in the hierarchy. The *dynamic real-time optimization* (DRTO) layer calculates optimal reference trajectories for the process, given constraints from the *scheduling and plantwide optimization* layer, as well as real-time data from the process. This layer typically operates on the time scale of hours. The calculated optimal reference trajectories are sent downwards to

the *advanced process control* layer, which contains the MPC application. This layer controls the process to follow the reference trajectories by, in the time scale of minutes, calculating new setpoints for the conventional PID-controllers in the *regulatory layer*. These PID-controllers are typically used to control properties like pressure, temperature, flow rate and composition, and they respond in the matter of seconds [27].

### 3 Process Description

Expandable polystyrene (EPS) is produced as a suspension in a semi-batch reactor, where reactants and additives can be fed during the reaction to obtain various effects on the product quality. A scheme of the process is shown in Figure 3.1. Because of the highly exothermic reaction nature, a cooling jacket is installed. The reactor content consists of styrene droplets dispersed in a continuous water phase. The reactor is stirred, and the agitation speed controls the size of the monomer droplets, and eventually, the size of the polymer beads of the product. An oil soluble chemical initiator, or commonly, a mix of several initiators, are added to the reactor.

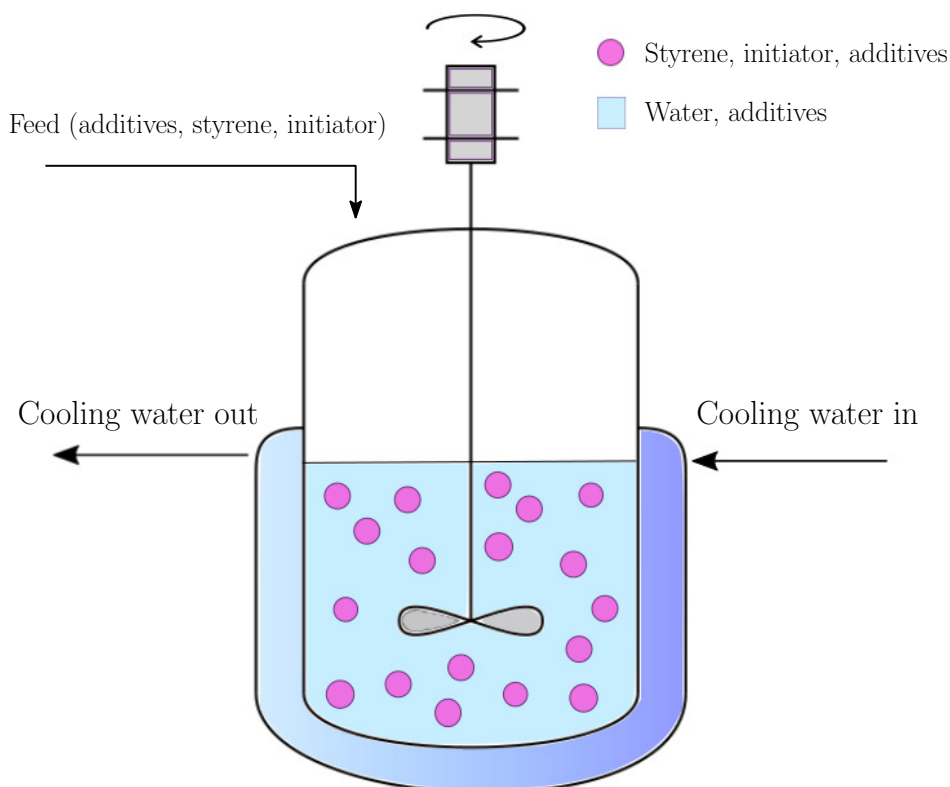


**Figure 3.1:** A semi-batch reactor for suspension polymerization of styrene.

Desired temperatures for polymerization of polystyrene are in the range of 100-140°C, and the polymerization temperature highly influences the final product [28].

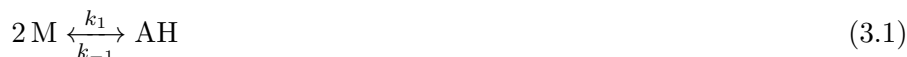
Various additives are usually needed in the process. Bead stabilizers are added to avoid aggregation of the dispersed phase. Aggregates could in the worst case scenario sink to the bottom of the reactor and give poor heat transfer conditions, resulting in thermal runaway. A blowing agent is also added while the reactions proceed. This is an oil soluble chemical that swells into the beads, and *n*-pentane is used for this purpose. When the EPS beads have reached the desired product quality and the polymerization process is terminated, the beads are heated

with steam. The blowing agent is then boiled off, giving air bubbles inside the polymer beads and expanding them to about eight times their initial size. The average bead diameter after expansion is approximately 1 mm [28].

### 3.1 Reaction Kinetics

Polystyrene is made by a free-radical polymerization process, where the development of long polymer chains from styrene building blocks is a result of radical reactions, as described in Section 2.1.

In the case of polystyrene, both chemical and thermal initiation occur. Chemical initiation proceeds as described in Section 2.1. Thermal initiation means that given sufficiently high temperature, styrene molecules will form radical components independently of additives to the process. The related reactions are shown in 3.1-3.4. In thermal initiation, two styrene molecules will undergo a Diels-Alder reaction and form the Diels-Alder adduct 1-phenyltetralin (AH) [29]. When the Diels-Alder adduct reacts with a styrene molecule, two radical molecules are formed, and these can further initiate a polymer chain.



Both the activation of a chain by a radical component from either thermal formation or chemical initiator decomposition, and the propagation reaction of a growing chain, are shown in Figure 3.2. In both cases, the free electron of the radical molecule forms a single bond with one of the electrons from the double bond of styrene. The result is the addition of a styrene molecule to the initiator radical or growing chain. Depending on the direction the styrene molecule approaches the radical, the phenyl group can point out of either side of the macromolecular backbone. Normal polystyrene is atactic, meaning that the order of the directions of the phenyl groups is random [30].

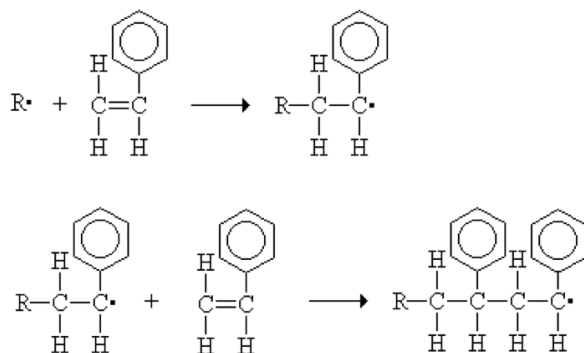


**Figure 3.2:** Activation of a new growing polystyrene chain and the propagation process.

Radical polystyrene chains mainly terminate through the termination by combination mechanism, and termination by disproportionation is negligible for production of EPS [29]. The most important chain transfer agent is monomer molecules [28]. In some cases, chemicals that acts as a CTA are added on purpose to control the chain length of the produced polymer [9].

Each of the organic phase droplets in the production of EPS can be considered a tiny lump of bulk polymerization, where diffusional limitations on the polymerization reactions is crucial. As the particles are swelled with pentane to obtain the expandability property of the beads, the viscosity of the liquid within each droplet is decreased. Hence, the amount of pentane added and the point in time when pentane is fed highly influences the physical properties of the finished bead product.

## 4 Modeling

This section will provide the assumptions made in the modeling work, the full mathematical description of the model and details on the implementation and solving of the model. The model is developed using the semi-batch reactor and polymerization modeling theory provided in Section 2.

### 4.1 Assumptions

To obtain a model with appropriate simplicity for optimization calculations and MPC, a series of assumptions are made for the process. It is important to notice that all of these assumptions are likely to contribute to an enlarged process-model mismatch, compared to a rigorous model that takes all involved phenomena into account.

First of all, the used chemical initiator will be different for different applications throughout this work, but it is always assumed that the chemical initiator is of the mono-functional kind.

Secondly, it is assumed that the reactor is charged with monomer and water, that the monomer is dispersed to tiny organic phase droplets in the continuous water phase, and furthermore that the reaction is initiated by adding all the chemical initiator at once at time  $t = 0$ . However, the model should give the possibility of also evaluating at the effects of feeding monomer and initiator during the batch. Feeding reactive components during operation gives extra degrees of freedom to control the reaction rate and temperature, as well as controlling the final product quality. Addition of pentane is assumed to start at some desired point during the reaction, and it is fed at a given rate over a short period of time.

There will most certainly be a delay between the addition of initiator and the onset of the initiation reaction. The same applies for the swelling of pentane into the particles. However, these effects are hard to quantify through measurements, and are therefore neglected. This means that no mass transfer limitations between the water phase and the polymer phase are considered in the model.

Further, the solubilities of styrene, initiator, polystyrene and pentane in water, and vice versa, are assumed to be negligible. Accordingly, there will be no water in the droplets of the polymer phase, and no styrene or pentane is lost to the water phase. In reality, styrene and pentane are slightly soluble in water, as shown in Table 4.1. This could result in a small amount of the added monomer not being available for reaction. Furthermore, some of the pentane is likely to be lost in the water phase, meaning that less pentane will contribute to reducing the diffusional limitation and the expansion properties of the polymer beads. In the same way, small amounts of water could dissolve in the polymer phase, increasing both its total and free volumes.

**Table 4.1:** Solubility of styrene, polystyrene and pentane in water, and vice versa, at 20 °C.

Compound	Solubility [kg/m <sup>3</sup> ]	Water solubility [kg/m <sup>3</sup> ]
Styrene [31]	0.29	0.54
Polystyrene [32]	0.00	0.00
Pentane [33]	0.40	0.09
Initiator (organic peroxides) [34]	0.00-0.01	0.00

Regarding the chemical reactions, all reactions are treated as elementary and irreversible. Rad-

ical chains are very reactive intermediate species, meaning that they are short-lived. Therefore, the pseudo-steady state assumption (PSSA) can be applied to the moment balances of living chains. This assumption is effective in eliminating the stiff condition of the differential equations originating from the radical dynamics [35].

When it comes to the energy balance, one important assumption is made. Since the polymer phase droplets are small and the reactor is vigorously mixed, mass transfer limitations between the polymer phase and the water phase are neglected. This means that the process is modeled completely without temperature gradients in the reactor content.

## 4.2 Dynamic Model Equations

Based on the assumptions discussed in Section 4.1, a dynamic model consisting of component balances for the reactor content and energy balances for the reactor vessel and the cooling jacket is formulated. All parameters used in the model equations are provided in Appendix A.

### 4.2.1 Component and Moment Balances

#### Component Balances:

Monomer (styrene) and initiator are both consumed in the reaction. These two reactants are added at the beginning of the batch ( $t = 0$ ), and in addition, they can be fed during the batch ( $t > 0$ ). As a base for the model with the purpose of primary testing and optimization, dicumyl peroxide (DCP) is chosen as the chemical initiator. For parameter estimation, this initiator is replaced with the initiator chemicals used to obtain the experimental data. The dynamic component balances for monomer and initiator are shown below.

$$\frac{dn_M}{dt} = R_M V + \hat{n}_M \quad (4.1)$$

$$\frac{dn_I}{dt} = R_I V + \hat{n}_I \quad (4.2)$$

$n_i$  is the amount of reactant  $i$  present in the system, and  $\hat{n}_i$  is the corresponding molar flow of the reactants.  $R_M$  and  $R_I$  are the reaction rates of monomer and initiator, respectively, and the expressions for these are shown in Equations 4.3 and 4.4 [36].

$$R_M = (-k_p - k_{trM})[M][\lambda_0] - 2fk_d[I] - 2k_{dm}[M]^3 \quad (4.3)$$

$$R_I = -2fk_d[I] \quad (4.4)$$

Here,  $k_p$ ,  $k_{trM}$ ,  $k_d$  and  $k_{dm}$  are the rate constants for propagation, chain transfer to monomer, initiation by chemical initiator and thermal initiation.  $f$  is the efficiency of the chemical initiator, which is a number between 0 and 1. Moreover,  $[I]$  and  $[M]$  are the concentrations of initiator and monomer, respectively, and  $[\lambda_0]$  is the zeroth order moment of active polymer chains on concentration basis.

The blowing agent, which in this case is pentane, is fed to the reactor at some point during the reaction, and does not contribute in any of the reactions. Hence, the balance equation for pentane is given by Equation 4.5. The amount of pentane ( $n_{C5}$ ) added to the system does, however, influence the volume and viscosity of the reactive phase.

$$\frac{dn_{C5}}{dt} = \hat{n}_{C5} \quad (4.5)$$

#### Moment Balances of Living and Dead Chains:

The moment balances are based on the work of Wu et al. [36], which handles a similar case of styrene polymerization. However, only thermal initiation is considered, and the moment balances are therefore extended with chemical initiation terms. In addition, PSSA is used for the radical chains, as mentioned in Section 4.1.

The zeroth order moment balance of living chains is defined in Equation 4.6. It represents the rate of change of the present amount of living chains. Active chains are produced by the two initiation processes, and they are consumed by termination. These reactions are represented by the three terms of Equation 4.6. The first order moment of living chains is related to the total chain length of all living chains. From the expression in Equation 4.7, it is clear that initiation and propagation increases chain length, while termination stops the growth. Transfer to monomer ends the growth of one chain, but initiates the growth of another. The balance equation for second order moments is shown in Equation 4.8, and is close to equivalent to the one for the first order moments, except that it balances the second order moments.

$$\frac{d\lambda_0}{dt} = (2fk_d[I] + 2k_{dm}[M]^3 - k_{tc}[\lambda_0]^2) V = 0 \quad (4.6)$$

$$\begin{aligned} \frac{d\lambda_1}{dt} = (2fk_d[I] + 2k_{dm}[M]^3 + k_{trM}[M][\lambda_0] + k_p[M][\lambda_0] \\ - k_{trM}[M][\lambda_1] - k_{tc}[\lambda_0][\lambda_1]) V = 0 \end{aligned} \quad (4.7)$$

$$\begin{aligned} \frac{d\lambda_2}{dt} = (2fk_d[I] + 2k_{dm}[M]^3 + k_{trM}[M][\lambda_0] + k_p[M](\lambda_0 + 2\lambda_2)) \\ - k_{trM}[M][\lambda_2] - k_{tc}[\lambda_0][\lambda_2]) V = 0 \end{aligned} \quad (4.8)$$

Since the PSSA is applied on the balances for living chains, the three equations above can be solved directly for  $\lambda_0$ ,  $\lambda_1$ , and  $\lambda_2$ . Consequently, these variables are calculated directly in the model.

The corresponding moment balances for dead chains are given in Equations 4.9, 4.10 and 4.11. The zeroth order moment increases when active chains are terminated, which can occur in the form of radical transfer to monomer and termination by combination. In the same way, the number of monomers tied in dead chains ( $\mu_1$ ) increase by the same termination processes. As for the living moments, the second order moment balance is similar to the first order moment balance, with an extra termination term.

$$\frac{d\mu_0}{dt} = \left( k_{trM}[M][\lambda_0] + k_{tc} \frac{[\lambda_0]^2}{2} \right) V \quad (4.9)$$

$$\frac{d\mu_1}{dt} = (k_{trM}[M][\lambda_1] + k_{tc}[\lambda_1][\lambda_0]) V \quad (4.10)$$

$$\frac{d\mu_2}{dt} = (k_{trM}[M][\lambda_2] + k_{tc}([\lambda_2][\lambda_0] + [\lambda_1]^2)) V \quad (4.11)$$

Rate constants:

The basic rate constants are calculated using a standard Arrhenius expression:

$$k_i = k_{i,0} \exp\left(-\frac{E_i}{RT_R}\right), i = \{d, dm, p, tc, trM\} \quad (4.12)$$

Here,  $k_{i,0}$  is the frequency factor,  $E_i$  is the activation energy and  $R$  is the gas constant.

As explained in Section 2.1, the initiation, propagation and termination reactions will eventually slow down due to diffusional limitations, and many strong models of these effects are based on free-volume theory. The model used in this work is based on the description given by Keer et al. [28].

In this model, the rate reduction of the three reactions are incorporated in the rate constants for the glass and gel effects, and in the initiator efficiency coefficient for the cage effect. All three effects are modeled using the free volumes of styrene, polystyrene and pentane, shown in Equation 4.13. In these equations,  $\alpha_i$  is fractional free volume,  $T_{g,i}$  is glass transition temperature and  $V_{m,i}$  is molar volume. The component index  $i$  represents either monomer, polymer or pentane.

$$V_{f,M} = (0.025 + \alpha_M(T_R - T_{g,M})) \frac{n_M V_{m,M}}{V} \quad (4.13a)$$

$$V_{f,P} = (0.025 + \alpha_P(T_R - T_{g,P})) \frac{\mu_0 V_{m,P}}{V} \quad (4.13b)$$

$$V_{f,C5} = (0.025 + \alpha_{C5}(T_R - T_{g,C5})) \frac{n_{C5} V_{m,C5}}{V} \quad (4.13c)$$

The total free volume of the reaction mixture is given by the sum of the contributions for each of the components, as shown in Equation 4.14.

$$V_f = V_{f,M} + V_{f,P} + V_{f,C5} \quad (4.14)$$

The gel effect is seen as the most important effect for the end product properties, and is included in most free-radical polymerization models proposed by research literature. In the free-volume theory model framework, the gel effect model is far more extensive than the ones for the cage and glass effects. The apparent termination rate due to the gel effect is in this model explained by three different diffusion regimes that contribute to diffusion control; segmental, translational and reaction diffusion.

At low monomer conversion and low viscosity of the reaction medium, *segmental diffusion* controls the diffusional limitations, and gives an increased termination rate at increasing conversion. The segmental diffusion-controlled termination rate constant is shown in Equation 4.15. For homopolymerization of styrene, this effect is very small, reflected in that the segmental diffusion parameter for styrene ( $\delta_c$ ) is close to zero [37].

$$k_{tc,seg} = \left[ 1 + \frac{\delta_c \mu_0 M_{w,M}}{V} \right] k_{tc} \quad (4.15)$$

At higher conversions, the *translational diffusion regime* starts to control the termination rate, and the termination rate constant for this regime is shown in Equation 4.16. Here,  $\bar{M}_{w,cr}$  and  $V_{f,cr}$  denotes the weight average molecular weight and free volume of the mixture at the onset of the translational diffusion effect.  $A$  and  $a$  are both tuning parameters.

$$k_{tc,trans} = \left( \frac{\bar{M}_w}{\bar{M}_{w,cr}} \right)^a \exp \left[ -A \left( \frac{1}{V_f} - \frac{1}{V_{f,cr}} \right) \right] k_{tc} \quad (4.16)$$

The onset of this regime is indicated by a critical point, where a test variable  $K$  becomes equal to a critical variable  $K_{cr}$ , both shown below. The test variable can be tuned by changing the two parameters  $l$  and  $A_l$ , and the critical variable can be tuned by changing  $A_{cr}$ .

$$K = \bar{M}_w^l \exp \left( \frac{A_l}{V_f} \right) \quad (4.17)$$

$$K_{cr} = A_{cr} \exp \left( \frac{E_{cr}}{RT_R} \right) \quad (4.18)$$

In addition, the *reaction* or *residual* diffusion contribution acts on the system at all conversions. As shown in Equation 4.19, the size of this effect is determined by a linear conversion function between an upper and a lower bound.

$$k_{tc,rd} = k_{trd,min} X + k_{trd,max} (1 - X) \quad (4.19)$$

The diffusional effects or regions can be gathered into one expression for the apparent termination rate:

$$k_{tc,app} = \left( \frac{1}{k_{tc,sec}} + \frac{1}{k_{tc,trans}} \right)^{-1} + k_{tc,rd} \quad (4.20)$$

For the cage and glass effects, much simpler models (shown in Equations 4.21 and 4.22) are used.

$$f_{app} = \exp \left[ -B \left( \frac{1}{V_f} - \frac{1}{V_{f,cr,d}} \right) \right] f \quad (4.21)$$

$$k_{p,app} = \exp \left[ -C \left( \frac{1}{V_f} - \frac{1}{V_{f,cr,p}} \right) \right] k_p \quad (4.22)$$

The critical free volumes are for these models predetermined known parameters  $V_{f,cr,d}$  and  $V_{f,cr,p}$ . Similarly as for the gel effect, the magnitude of the effects can be changed by manipulating the tuning parameters  $B$  and  $C$ .

### 4.2.2 Energy Balances

The energy balance of the reactor vessel is developed on the form of a temperature equation as discussed in Section 2.2.1, and the more specified equation for the considered system becomes:

$$\frac{dT_R}{dt} = \frac{\sum_i c_{p,i} \hat{n}_i (T_{feed} - T_R) - \Delta H_R R_p V - (UA)_J (T_R - T_J) - (UA)_{amb} (T_R - T_{amb}) + W_{ag}}{\sum_i n_i c_{p,i} + m_v c_{p,v}} \quad (4.23)$$

Here, the first term is equivalent to the enthalpy stream term from Section 2.2.1, and  $T_{feed}$  is the temperature of the feed. For free-radical polymerization, the bulk of the reaction heat generated originates from the propagation reaction, and therefore, the propagation rate  $R_p$  is used in the heat of reaction term. The propagation rate depends on the concentrations of monomer and living polymer chains, and the expression is shown in Equation 4.24.

$$R_p = k_p [M] [\lambda_0] \quad (4.24)$$

The heat term  $Q$  is replaced by the heat loss to the cooling jacket and the surroundings of the reactor. In these terms  $(UA)_J$  and  $(UA)_{amb}$  are the overall heat transfer coefficients for heat transfer to the cooling water and surroundings, respectively.  $T_J$  and  $T_{amb}$  denotes the cooling fluid and ambient temperatures. The shaft work is in this case the work done on the system by agitation,  $W_{ag}$ .

As the cooling provided by the cooling system is dependent of the temperature of the cooling water, an energy balance or temperature equation for the cooling jacket must also be a part of the model. For this case, it is given by the following:

$$\frac{dT_J}{dt} = \frac{(UA)_J (T_R - T_J) + \hat{m}_c c_{p_c} (T_{J,i} - T_{J,o})}{m_c c_{p_c}} \quad (4.25)$$

, where  $\hat{m}_c$  is the flow rate of cooling fluid,  $c_{p_c}$  is the heat capacity of the cooling fluid,  $T_{J,i}$  and  $T_{J,o}$  are the inlet and outlet temperatures of the jacket, respectively, and  $m_c$  is the mass of cooling fluid contained in the jacket.

### 4.3 Model Structure and Choice of Model Variables

The model as a whole is structured on the following form:

$$\dot{x}(t) = f(t, x(t), u(t), \theta) \quad (4.26a)$$

$$x(0) = \text{given} \quad (4.26b)$$

$$y_p(t) = g(t, x(t), u(t), \theta) \quad (4.26c)$$

$$z(t) = h(t, x(t), u(t), \theta) \quad (4.26d)$$

Here,  $x$  is the state vector,  $u$  is the input vector,  $\theta$  is the vector of parameters,  $y_p$  is the vector of (predicted) measurement variables and  $z$  is the output vector.

Since the modeling objective in this case is to perform an offline batch optimization related to product quality and batch time, the required set of variables is small compared to the modeling objective of full reactor operation and control. This would for instance include pressure control

of the reactor. In operation, pressure control is necessary, but early research have shown that the conversion rate and product quality of polystyrene is not significantly influenced at pressures lower than 1000 atm [38].

The differential equations in vector form (Equation 4.26a) are the same as the model equations shown in Sections 4.2.1 and 4.2.2. The states are the balanced variables in these equations, meaning the present amounts of monomer and initiator, the moments for dead chains and the reactor and jacket temperatures. The moments of living chains are included into the output vector, since the calculation of these does not require solving of differential equations.

As input variables, it is natural to choose the flow rates of monomer, initiator and pentane into the reactor, as well as the flow rate of cooling fluid. However, to ensure the possibility of perfect temperature control, an extra input variable related to temperature is included ( $dT_R$ ). Perfect temperature control is useful both for comparing the model results to measurement data in parameter estimation and model validation, and for performing optimization calculations. As the manipulated variable for perfect temperature control and optimization, the reactor temperature derivative is chosen. This provides a smooth temperature trajectory, compared to directly manipulating the temperature, as a new temperature can only be determined at each sampling instant.

For a real reactor system, the available measurements of the system would be given, and these would be a reasonable starting point for choosing measurement variables for the model. Since this project work is not related to a specific semi-batch reactor for styrene polymerization, only the essential measurements are included in the model framework. These include measurements of the reactor and jacket temperature, as well as measurements of the weight and number average molecular weights.

As already mentioned, the moments of living chains are directly calculated from the states, and therefore belong in the output vector. The average molecular weights are also included in the output vector for possibility of comparison between measurements and model predictions. In addition, other variables that are calculated from the states and inputs and tell something about the progress or product of the semi-batch process are included. These are number average chain length, conversion, polydispersity index and cooling demand to keep the desired reactor temperature. The calculation procedure of these variables are explained in Section 2.3.

To summarize the choice of state, input, measurement and output variables, the elements of the various vectors are shown below.

$$x = \begin{bmatrix} n_M \\ n_I \\ n_{C5} \\ \mu_0 \\ \mu_1 \\ \mu_2 \\ T_R \\ T_J \end{bmatrix} \quad u = \begin{bmatrix} \hat{n}_M \\ \hat{n}_I \\ \hat{n}_{C5} \\ \hat{n}_c \\ dT_R \end{bmatrix} \quad y_p = \begin{bmatrix} T_{R,p} \\ T_{J,p} \\ \bar{M}_{n,p} \\ \bar{M}_{w,p} \end{bmatrix} \quad z = \begin{bmatrix} \lambda_0 \\ \lambda_1 \\ \lambda_2 \\ \bar{M}_n \\ \bar{M}_w \\ \bar{n} \\ X \\ PI \\ Q_{J,d} \end{bmatrix} \quad (4.27)$$

## 4.4 Implementation and Numerical Solving of the Model

The model is formulated in the programming language C using a model template. This template gives a framework for the model which is recognized by Cybernetica's various software applications. In this framework, variables of the different types (states, inputs, measurements, outputs, parameters and constants) are declared, and the model equations are formulated in functions. The framework also contains functionality for solving the model, as well as interfaces between the model and other applications such as Cybernetica ModelFit and Cybernetica CENIT.

Four different numerical solution methods are built in. The simplest is Euler integration, which is the one used to solve the model given in Section 4.2. The differential equations in concern are on the form of Equation 4.28a, and the initial conditions for the states are given. Then, Euler's Method for solving this system is given by Equation 4.28c.

$$\dot{x}(t) = f(t, x(t), u(t), \theta) \quad (4.28a)$$

$$x(t_0) = x_0 \quad (4.28b)$$

$$x_{k+1} = x_k + \Delta t_{int} f(k, x_k, u_k, \theta) \quad (4.28c)$$

Euler's Method is chosen as the numerical solver in this case because it is fast and sufficiently accurate for the model in concern with a relatively large step length. This is possible due to the numerical robustness of the model. The sampling time  $\Delta t$  of the model is chosen to be 15 seconds, and the integration time step  $\Delta t_{int}$  is chosen to be equal to the sampling time. Shorter step lengths and more sophisticated solvers, using a variable step length that adjusts for dynamic variations in the solved differential equations, have also been tested for the model. The conclusion from this investigation is that using more advanced methods and shorter step lengths increases computation time, and gives little contribution to simulation accuracy. However, for a case where PSSA is not applied on the living chain reactions, such measures are unavoidable due to the stiff conditions of the differential equations.

## 4.5 Results and Discussion

This section presents simulation results of the model. First, the effects of constant temperature and initiator addition on the product quality, polymerization time and diffusional limitations on the reactions, are investigated in Section 4.5.1. Further, the effect of pentane addition on diffusional limitations and the resulting product quality is handled in Section 4.5.2.

### 4.5.1 Effect of Temperature and Monomer to Initiator Ratio

The dynamic development of number and weight average molecular weights, monomer conversion, initiator consumption and efficiency, and propagation and termination rate constants for different constant temperatures and initiator amounts are shown in Figures 4.1-4.7. The initial monomer amount is for simplicity set to 1 mol, and the total simulation time is 225 minutes. The model is simulated at the temperatures 100, 120 and 140 °C, and monomer to initiator ratios 50, 100 and 200.

It is seen from Figure 4.1 that  $\bar{M}_n$  is strongly dependent on both the temperature and the initiator concentration. In the given temperature range, the final product number average molecular weight varies from slightly above 150 kg/mol for the lowest temperature, down to 20 kg/mol for the high temperature case. This implies that, according to the model, even a small temperature change alters the product quality. Also the varying initiator content gives a large range of product qualities.

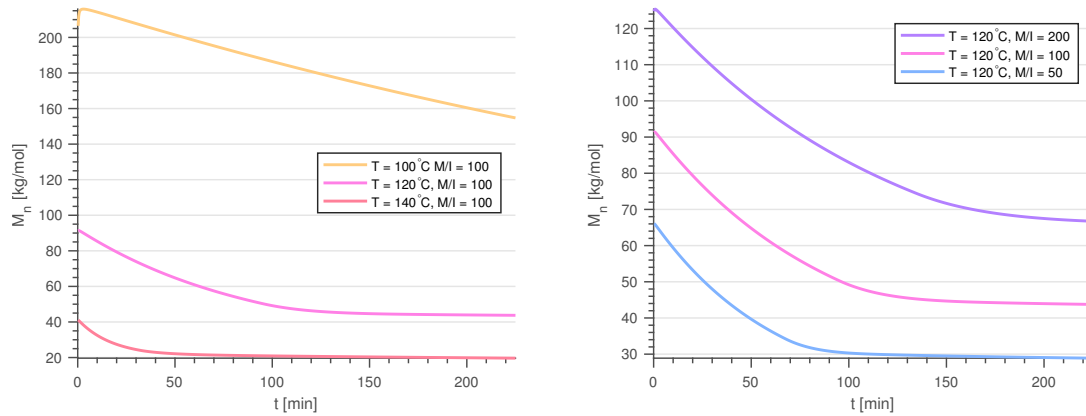


**Figure 4.1:** Number average molecular weight simulation results.

It is expected that average molecular weight in general is reduced with increasing temperatures and initiator amounts. At high temperatures, the initiation and termination reactions are more dominant than the propagation reaction, resulting in shorter chains. The high initiator content has the effect of activating more chains, and as a result the available monomer molecules are spread on more and shorter chains. In addition to the varying values of the final  $\bar{M}_n$  between different reactor conditions, the value of  $\bar{M}_n$  settles at a constant value at different points in time for the various conditions. Polymerizations at high temperatures and large initiator amounts have the tendency of settling at a constant level early. This behavior is connected to the conversion rate, which will be discussed in further detail in the following.

The weight average molecular weight development in Figure 4.2 follows the exact same trends as the ones seen in Figure 4.1. However,  $\bar{M}_w$  takes much larger values than  $\bar{M}_n$  for the same reactor conditions. It should also be noted that the ratio between the two average molecular weights are not constant, meaning that polymers with different polydispersity are produced within the range of temperatures and recipes.

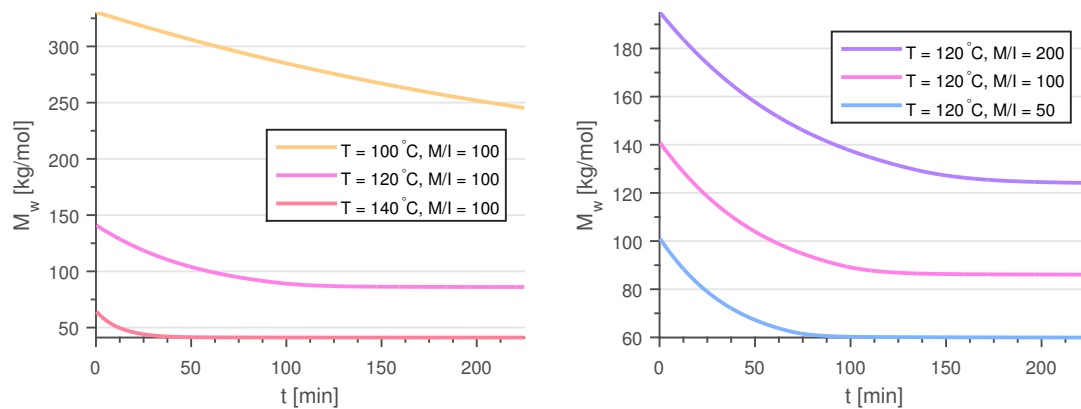


**Figure 4.2:** Weight average molecular weight simulation results.

In the reactor condition ranges at hand, the styrene conversion development is especially sensitive to temperature changes. For high temperatures ( $T_R = 140^\circ\text{C}$ ), the conversion curve is very steep at the beginning of the batch, leveling out on 100% conversion towards the end of the batch. For the  $100^\circ\text{C}$  case, the conversion shows a more linear development with respect to time, ending up at only 60%. This is expected, as all reactions involved in free-radical polymerization are slower at lower temperature, as indicated by the temperature sensitivity in the Arrhenius expression given in Equation 4.12. The variations in the initiator amount between 0.005 and 0.02 mol also result in different conversion rates. Larger amounts of initiator initially charged to the reactor give a slightly larger conversion rate in the first few minutes, resulting in a higher end conversion. This behavior is also according to expectations, as more initiator present will result in a higher number of active chains which can bind free monomer molecules in the reaction mixture.

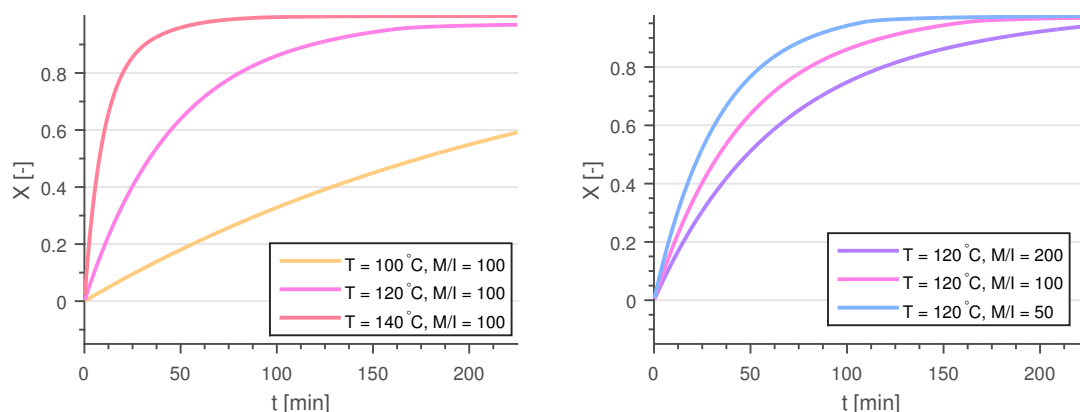


**Figure 4.3:** Styrene conversion simulation results.

The initiator consumption is, similarly to the monomer conversion, highly dependent on the reaction temperature. The development of the initiator content in the reactor for the different simulated cases are shown in Figure 4.4. For the high temperature case, close to all of the added initiator is consumed, while for lower temperatures, residual initiator is present in the end product. For the lowest temperature, barely any initiator is consumed, meaning that the few chains present have grown long. This theory is confirmed by considering the number and weight average molecular weights for this case, which take significantly larger values compared to the other cases.

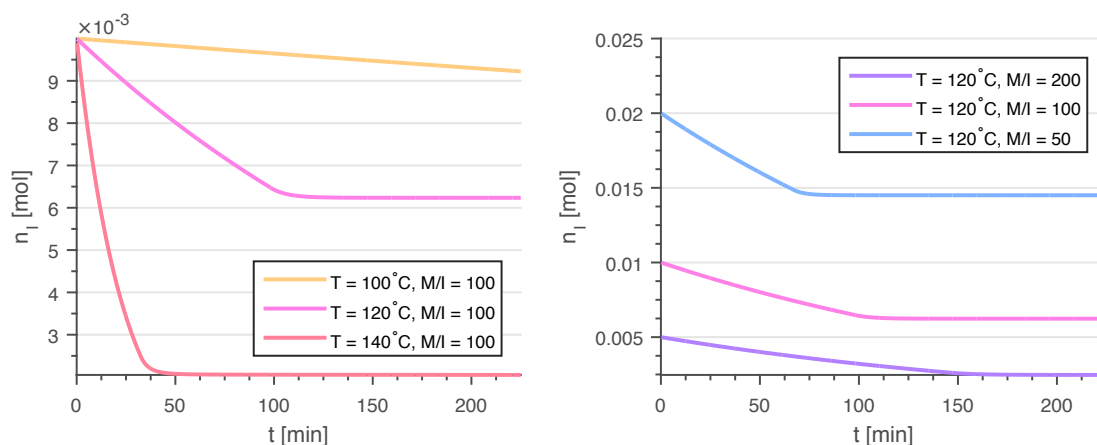


**Figure 4.4:** Initiator content simulation results.

Most of the initiator consumption curves have a more or less sharp breakpoint. To understand why these appear, Figure 4.5 must be considered. Because of the increasing viscosity of the polymer phase, the cage effect will cause the apparent initiator efficiency to decline at a point where the free volume of the reaction mixture has reached a critically low value. This behavior is clearly seen in the figure below. For high temperatures and large initiator amounts, the polymerization rate is faster, meaning that the free volume reaches a critical value earlier, resulting in the onset of the cage effect. For the lowest temperature case, the polymerization rate is so slow that the reaction mixture never reaches the critical point within the simulation time frame of 225 minutes. When comparing Figure 4.4 to Figure 4.5, it is seen that the onset of the cage effect is causing the breakpoints in the initiator content dynamics.

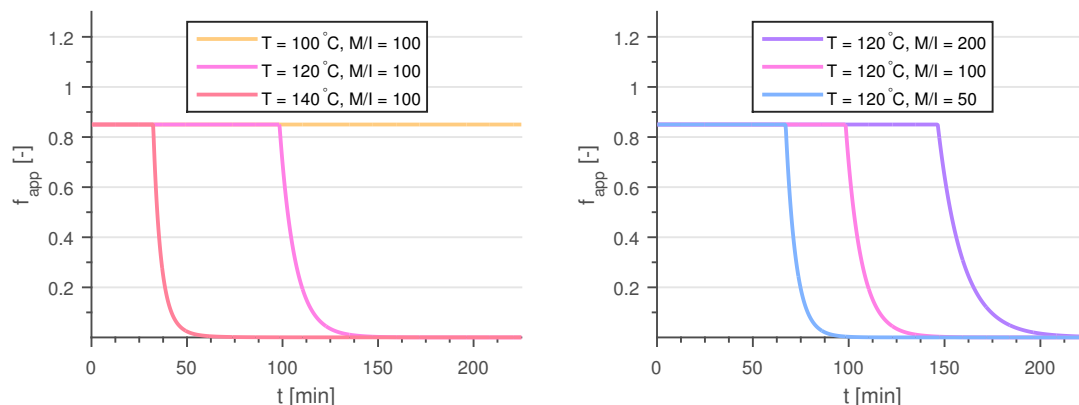


**Figure 4.5:** Apparent initiator efficiency simulation results.

The apparent propagation rate for the different simulated reactor conditions are shown in Figure 4.6. Some of the conditions show an onset of the glass effect during the simulated time period. The lowest temperature and initiator amount is according to the model not affected by diffusional limitations on the propagation reaction. Increasing temperatures and initiator addition results in earlier onset of the glass effect. This is due to the same reason as for the onset of the cage effect. Conditions causing fast polymerization also gives higher viscosity at an earlier stage.

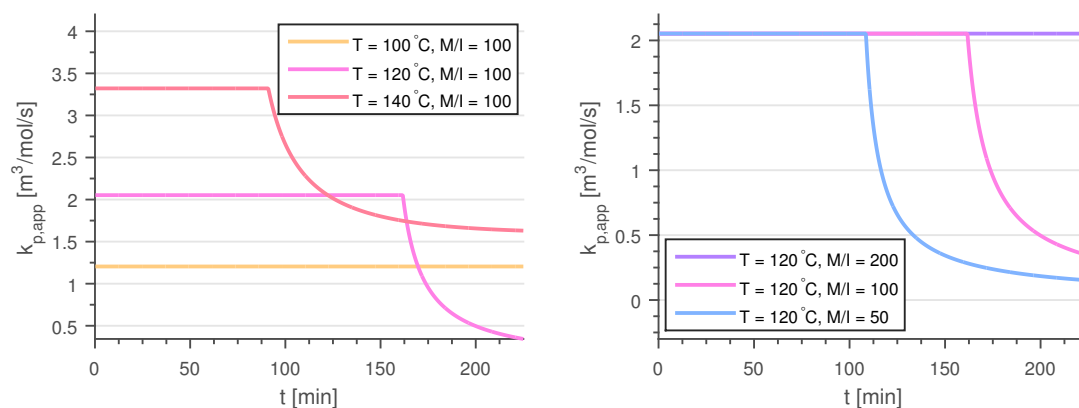


**Figure 4.6:** Apparent propagation rate constant simulation results.

Similarly, the apparent termination by combination rate constant, given in Figure 4.7, is showing the same kind of behavior due to the gel effect. The magnitude of the drop in the termination

rate constant is large compared to the changes in the apparent initiator decomposition rate and propagation rate caused by the cage and glass effects. This explains why the gel effect is seen as a far more extensive effect when it comes to impact on the product quality.

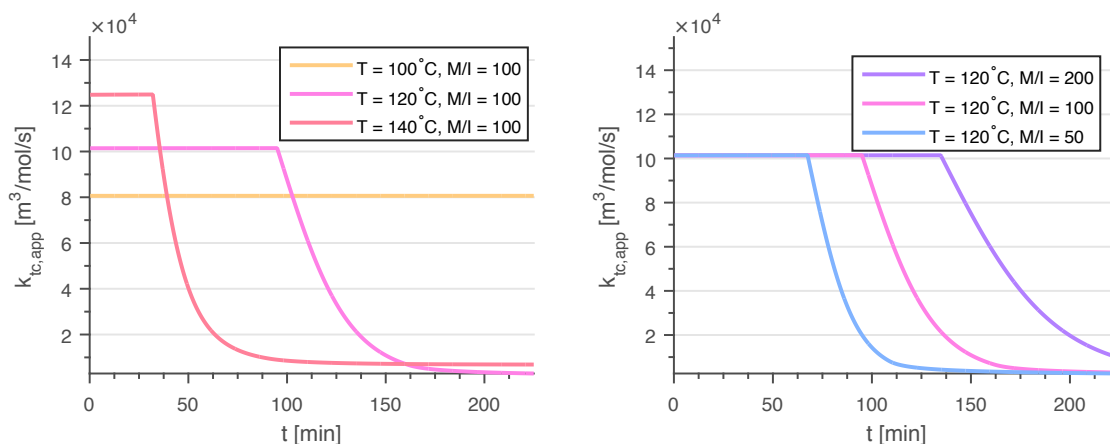


**Figure 4.7:** Apparent termination by combination rate constant simulation results.

From these results, it can be concluded that the qualitative behavior of the model, given differences in reactor temperature and initially loaded initiator, is in accordance with expectations. Increasing temperature and initiator concentration both result in faster polymerization and shorter chains, which is in line with statements from literature. In conditions that generate heavy polymerization in an early stage of the process, diffusional limitations on the reactions in the form of the glass, cage and gel effects are present. It should be noted that the modeling approach of these effects assumes that the three effects act in the same manner. It also assumes that these effects arise at a critical point, and that the reaction rate falls exponentially after this point. These assumptions could be said to give a very simple representation of the real mechanisms and behavior of the diffusion limited reactions.

#### 4.5.2 Effect of Pentane

As stated in Section 2.3.4, additions of low viscosity liquids such as pentane will reduce the impact of the cage, glass and gel effects by introducing new free volume between the reacting molecules. Figures 4.8-4.10 show relevant simulations of apparent rate constants and initiator efficiency, number and weight average molecular weight and monomer conversion and initiator content, given different amounts of pentane. The other reaction conditions are the same as the base case considered in Section 4.5.1, with a reactor temperature of 120 °C and monomer to initiator ratio equal to 100. The different pentane amounts used in the simulations are 0.014, 0.07 and 0.14 mol of pentane present from the beginning of the batch process. These pentane amounts correspond to 3.6, 18 and 36 wt%, respectively.

The apparent termination rate, propagation rate and initiator efficiency are shown in Figure 4.8. The development in these show that the model has the ability to produce the expected delay in the gel, glass and cage effects from addition of low viscosity pentane. The more pentane added, the stronger is the reduced viscosity effect. For the largest pentane addition of 36 wt%, all diffusional limitations on the polymerization reactions are completely removed. With 18 wt% pentane added from the beginning, the gel and cage effects are clearly delayed compared to the case with only a very small portion of pentane, and the glass effect is removed.

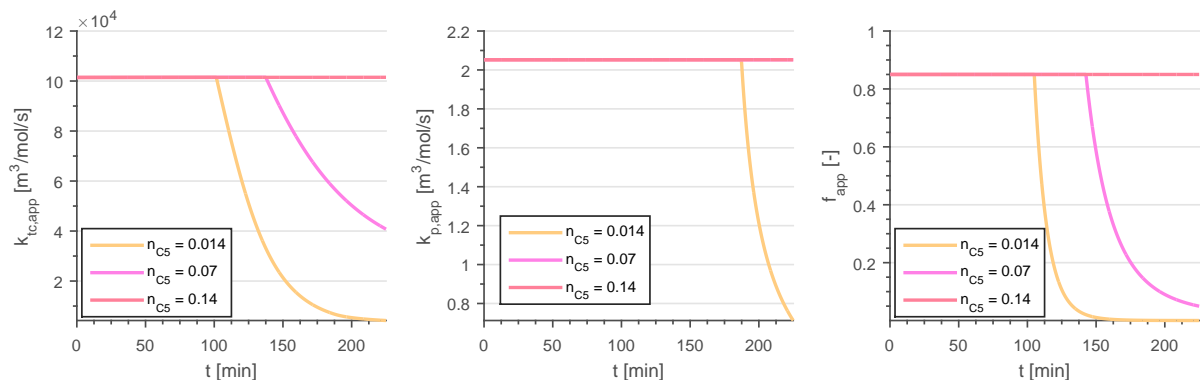


**Figure 4.8:** Apparent termination and propagation rate constants and initiator efficiency simulation results for different amounts of pentane added.

The number and weight average molecular weight developments, shown in Figure 4.9, are relatively similar between the different pentane additions during the first part of the batch. In this region, the gel, glass and cage effects have not been activated, and the molecular weight difference is due to changes in the reaction volume itself. However, when the low pentane case enters the critical region, one can clearly observe that the end product quality in terms of the molecular weight is changed. The final number and weight average molecular weights are reduced with increasing pentane addition, because of the inhibition of the gel effect which reduces the termination rate and gives longer chains.

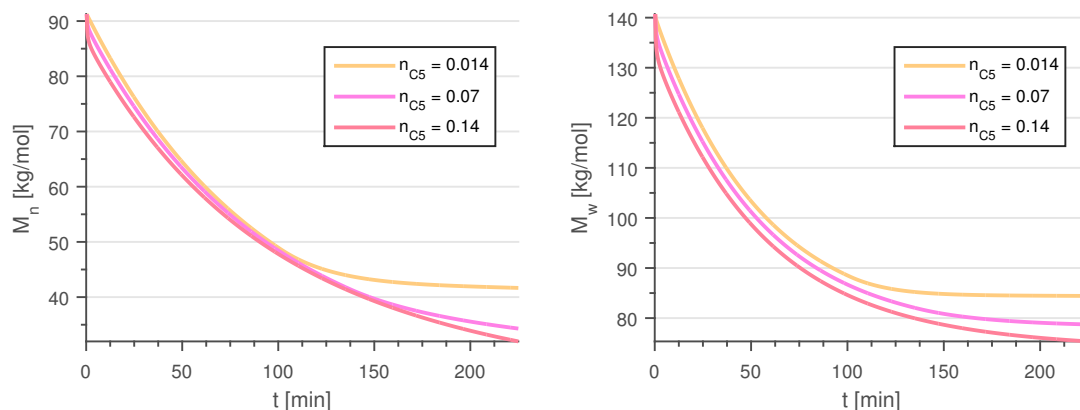


**Figure 4.9:** Number and weight average molecular weight simulation results for different amounts of pentane added.

The styrene conversion and initiator contents of the reactor in terms of changes throughout the batch process are shown in Figure 4.10. The conversion shows very little sensitivity to the pentane addition. As the glass effect is clearly influenced by the pentane addition, this means that the magnitude of the propagation rate change is so small that the glass effect is barely seen on the conversion rate. It is rather hard to say whether or not this result is in agreement with real free-radical polymerization processes. Results from similar experiments of bulk polymerization of styrene in presence of pentane published by Villalobos et al. in 1993 indicates that the pentane sensitivity of the conversion variable is too low in the model [37]. In the work by Villalobos et al., pentane additions of 0, 7.5 and 15 wt% give a clearly observable difference both in the conversion rate and the end conversion after 480 minutes of polymerization. On the other hand, the cage effect has an apparent effect on the initiator decomposition rate from

the moment of entering the critical region. This is seen as breakpoints, similar to the ones seen in Section 4.5.1, in the initiator consumption curves at the time when the apparent initiator efficiency starts to fall.

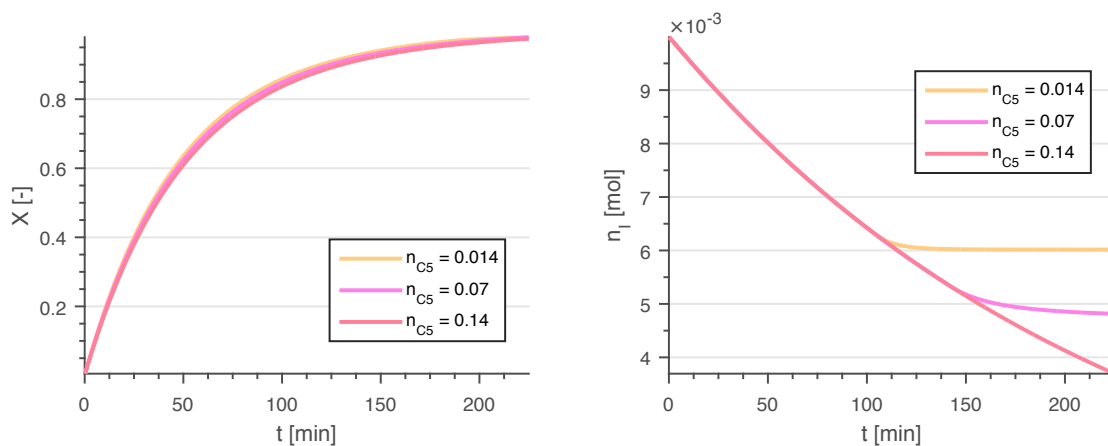


**Figure 4.10:** Monomer conversion and initiator consumption simulation results for different amounts of pentane added.

From these results, it is clear that the model is at least qualitatively able to reproduce the theoretical basis on diffusional limited reactions and presence of a low viscosity medium in the reaction mixture. As expected, all of the three effects are delayed, faded or completely removed in the considered time frame, when pentane is present from the point of initiation. However, comparison with experimental results from similar polymerization processes indicates that the sensitivity to pentane addition might be underestimated by the model.

## 5 Offline Parameter Estimation

The parameter estimation of the model described in Section 4 is performed using Cybernetica Modelfit, a software program developed by Cybernetica AS. ModelFit is built for recognizing the components of a model written in the C template used to implement and solve the EPS semi-batch reactor model. It contains features for simulation and offline parameter estimation. There are also embedded algorithms for running recursive parameter and state estimation in the form of an EKF. As the input plant measurements, Cybernetica Modelfit uses logged time-series data from the plant, and solves a similar optimization problem as shown in 2.17 [15].

The set of parameters to estimate is determined by the user, and as a useful tool in deciding which parameters to choose for estimation, ModelFit provides an *identifiability ranking*. *Identifiability* is defined as the theoretical ability to learn the true underlying parameter values of the model [39]. How identifiable a set of parameters are, is affected by the cost function’s sensitivity to the parameters and the linear dependence between the parameters.

In this work, the parameters chosen for estimation are:

$$\eta = \begin{bmatrix} k_{0,p} \\ k_{0,trM} \\ k_{0,tc} \\ E_p \\ E_{trM} \\ E_{tc} \\ A_{cr} \end{bmatrix} \quad (5.1)$$

The frequency factors for propagation, transfer to monomer and termination are chosen to adjust the magnitude of the reaction rates. The activation energies for the same reactions are chosen to adjust for the temperature dependency implied by the plant measurements. Note that both chemical and thermal initiation is excluded from this set. This is due to the linear dependency between these two variables, and the termination by combination rate, indicated by the identifiability ranking provided by ModelFit. Hence, it is not possible to choose these variables for estimation simultaneously. Finally, the frequency factor of the critical variable  $K_{cr}$  is estimated to adjust the onset of the gel effect.

### 5.1 Results and Discussion

The parameter estimation has been performed for a given recipe and reactor conditions, using measurement data provided by a major European polymer producing corporation. The reactor conditions in the form of a temperature profile and the timing for pentane addition is shown in Figure 5.1. The axes have been scaled due to confidentiality of the given reactor conditions. The time axis is scaled by the total batch time, the temperature profile is scaled by the initial temperature and the pentane addition is scaled by the total added pentane amount in the end of the batch.

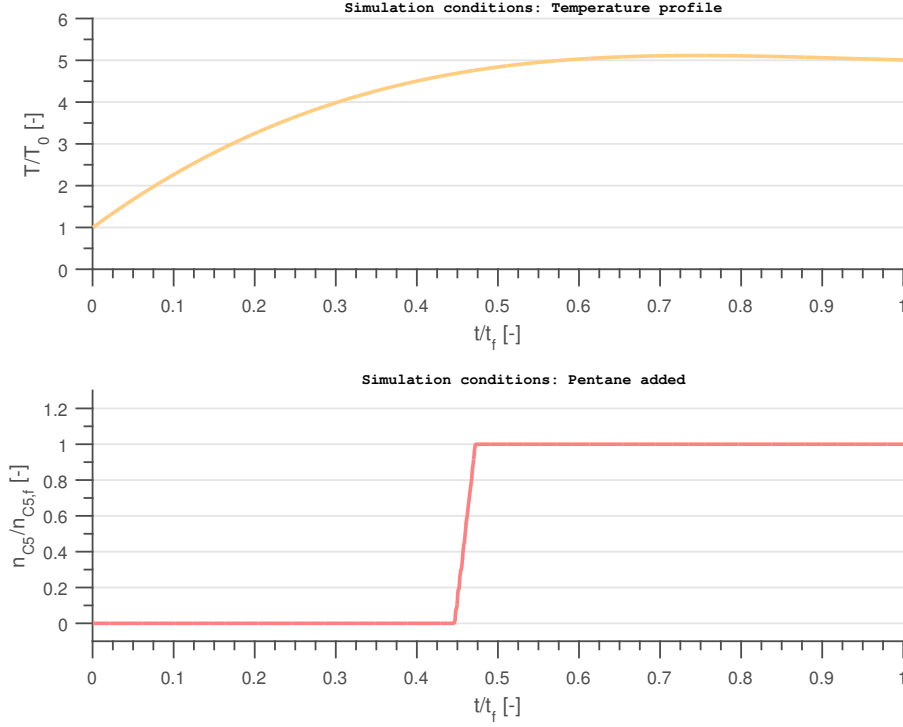


**Figure 5.1:** Temperature profile and pentane addition for parameter estimation.

The offline parameter estimation calculation gave increased values for  $k_{0,p}$ ,  $k_{0,ktM}$ ,  $E_p$  and  $A_{cr}$  and reduced values for  $k_{0,tc}$  and  $E_{tc}$ . The value for  $E_{trM}$  was held constant. According to this optimization calculation, it is more optimal to choose a lower value for the termination by combination frequency factor and in addition decrease the temperature sensitivity, and increase the total value of the termination rate constant, by reducing  $E_{tc}$ . This change has the effect of increasing the overall termination rate, which especially reduces the initial molecular weights. The enlarged transfer to monomer frequency factor also has the effect of reducing the molecular weight in the form of terminating longer chains in order to start new ones. To balance the increased termination, the propagation rate is significantly increased by raising the value of  $k_{0,p}$  and slightly increasing its sensitivity to temperature by changing  $E_p$ . The critical gel effect factor  $A_{cr}$  is increased, meaning that the onset of the gel effect should occur later in time, according to the offline parameter estimation. This change has the effect of reducing  $\bar{M}_n$  in the end of the batch.

The obtained results are shown in Figures 5.2 and 5.3. Here, plant measurements and model predictions before and after parameter estimation are shown for weight and number average molecular weight, respectively. The quality axes are here scaled by the quality measurements at the end of the batch ( $\bar{M}_{w,m,f}$  and  $\bar{M}_{n,m,f}$ ).

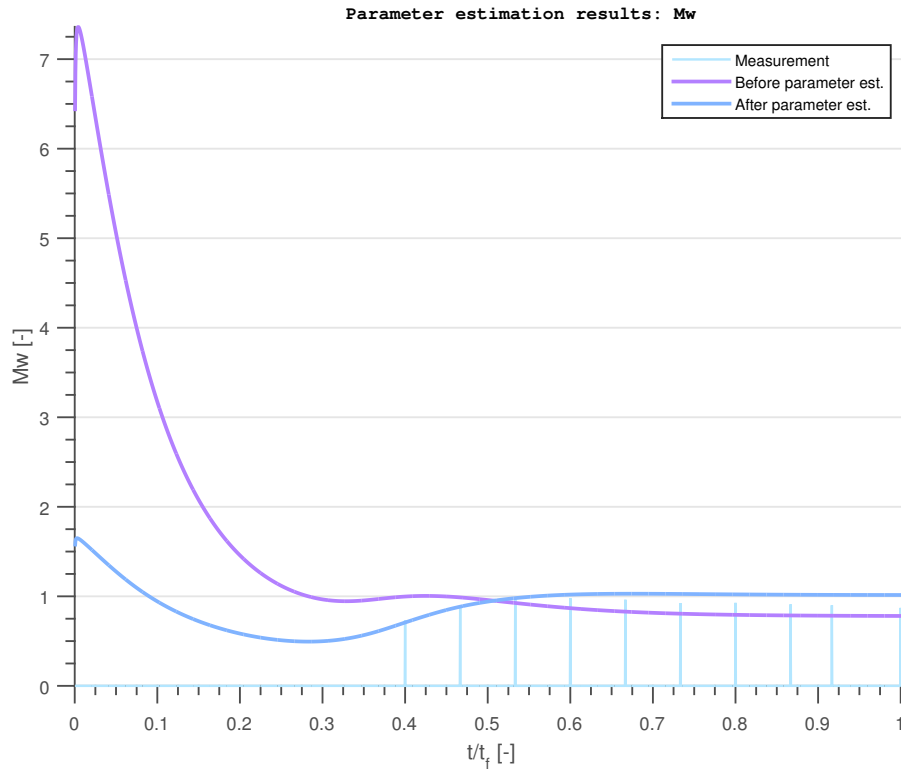


Figure 5.2:  $\bar{M}_w$  measurements and model predictions before and after parameter estimation.

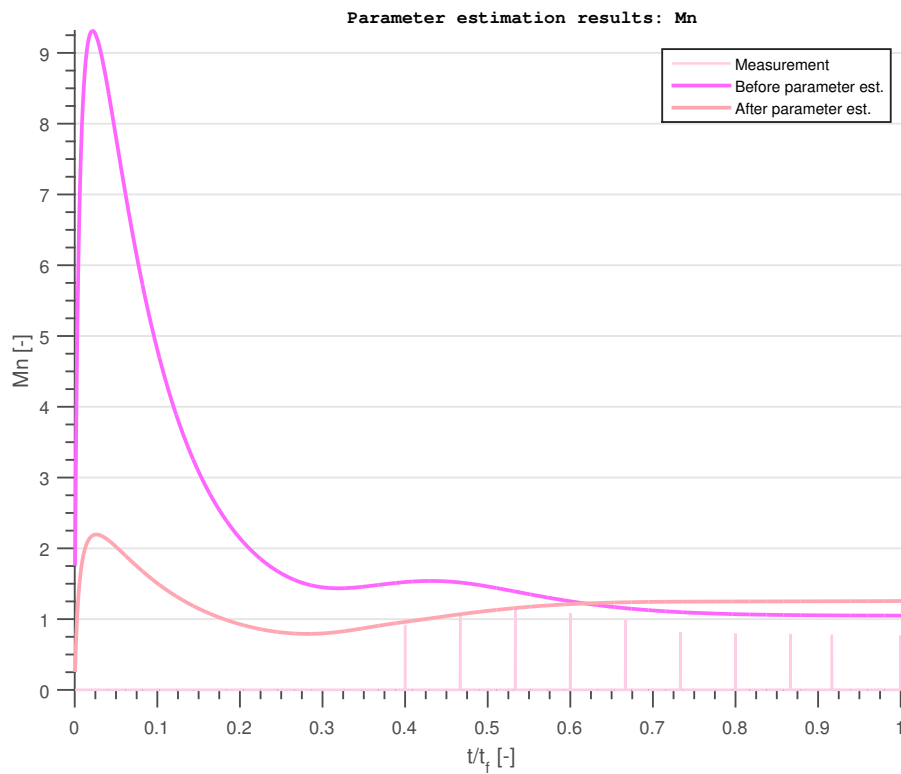


Figure 5.3:  $\bar{M}_n$  measurements and model predictions before and after parameter estimation.

As seen from both plots, the model with parameters from literature fails to restore the trend of the first measurements, taken from when the process has reached 40% of the batch time. The model with estimated parameters shows improvement for both  $\bar{M}_w$  and  $\bar{M}_n$  in producing the dynamics of the first measurements. However, the accuracy of predicting the final product quality does not seem to increase. In Figure 5.3, this is especially visible, as the predicted number average molecular weight is significantly higher than the measurement values.

The available basic data for parameter estimation is in this case very limited. Only a few data points are logged, and they are all placed in the last half of the batch time horizon. This means that it is impossible to say which of the initial behaviors shown by the pre- and post parameter estimation models is the closest to reality. Also, the logged measurement data set lack data from different reactor conditions, such as temperatures and initiator amounts.

It is also important to note that a measure on the uncertainty of the measurements is not given. This means that it is assumed that all measurement points are able to completely and truly describe the state of the system at the given point in time, which is a rather rough assumption. Uncertain measurements could result in poor quality of the estimated parameters. In this case, an online parameter estimation combined with state estimation would produce a better fit.

The conclusion from this work is that in order to obtain better qualitative fit between the model and the plant, parameter estimation using a more complete set of data is necessary.

## 6 Optimization

The increasing competition in the chemical industry has established the need of economically optimal operation and flexible production plants. The polymer industry and production of expandable polystyrene are no exceptions [40]. A case study from 2013 on the necessary measures for EPS manufacturers to remain competitive states that plant capacity utilization is key to reduce production cost and maximize profitability [3].

For an EPS production plant, plant capacity utilization is mainly connected to *i*) run as many batch processes as possible at the same time, and *ii*) limit the amount of time spent on each batch run. The amount of EPS produced per time unit in an EPS production plant is predominantly limited by the available cooling water capacity. As previously mentioned, sufficient cooling of the reactor is crucial to avoid thermal runaway and to remain at safe operation of the reactor, as well as attaining the desired product quality. The cooling capacity is time-varying, as the availability of water and the water temperature can vary throughout the year.

### 6.1 Plantwide Optimization of EPS Production

A diagram showing a possible hierarchical structure for the EPS plant, similar to the one discussed in Section 2.7, is given in Figure 6.1. On the top level, *plantwide optimization*, decisions depending on the current market demands of EPS and the availability of resources such as reactants and cooling water are made. This layer has the responsibility of distributing resources to the batch reactors in the plant in an optimal manner. This information is passed to the DRTO layer as constraints. The DRTO layer then solves an optimization problem based on the given constraints and measurements from the process. The solution to this optimization problem is optimal trajectories for the controlled variables, given the objectives of optimal operation, meaning to obtain the desired product quality in the least amount of time. The optimal output and input trajectories are then passed to the NMPC layer, which seeks to control the process close to the optimal paths.

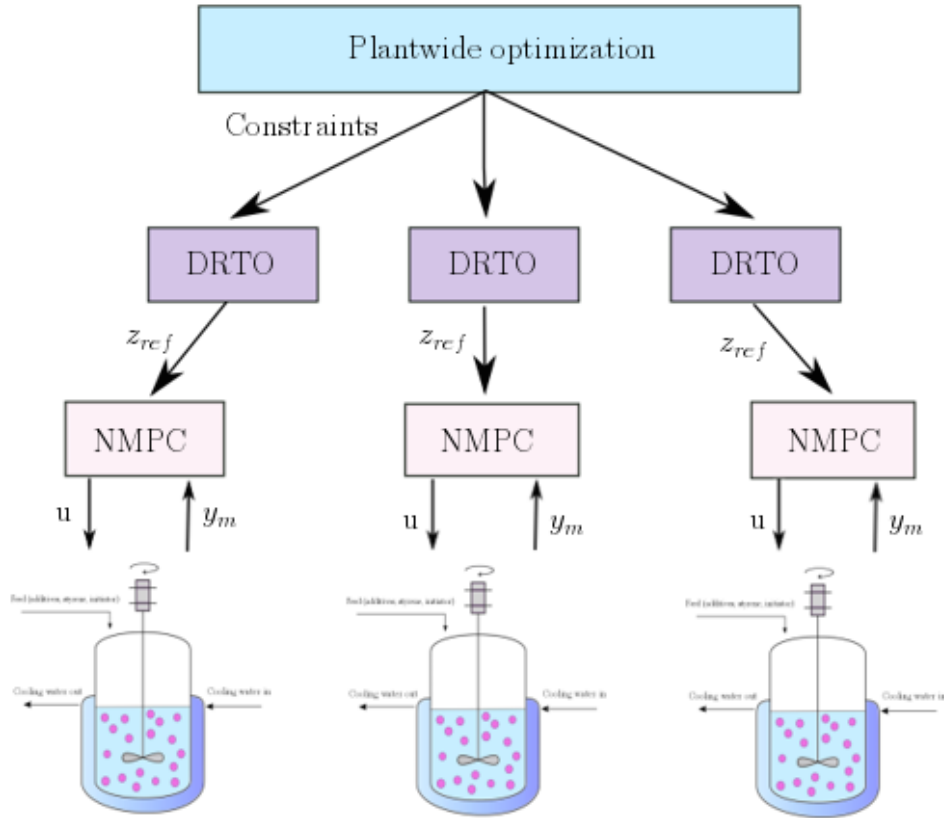


**Figure 6.1:** Diagram of plantwide optimization of an EPS polymerization plant.

The aim of this work is to formulate an optimization problem and solution method for offline optimization of the semi-batch process. Because optimizing the entire plant in order to improve plant utilization is interesting in an economical perspective, this offline optimization procedure could act as a pre-stage of a DRTO application. This DRTO layer would re-optimize trajectories based on information from the process and modified constraints from the plantwide optimization layer.

## 6.2 Formulation of the Optimization Problem

The aim of the optimization is to reduce the batch time required to reach the desired product quality and conversion. At the same time, the cooling demand must stay below or on the available cooling capacity. For the purpose of this study, product quality is assumed to be determined only by the number average molecular weight, meaning that the weight average molecular weight varies according to the model. The used decision variables are the initial ratio between loaded monomer and loaded initiator, as well as the dynamic temperature trajectory during the batch. Addition of pentane is not taken into consideration for this part of the work.

There are many possible optimization problem formulations that seek to fulfill these goals, and the chosen formulation is shown in Equation 2.19. The choice of such a problem formulation is built upon many engineering decisions; prioritizing between the different goals and determining

for which variables deviations from the desired values can be accepted.

$$\min_{T_{R,0}, dT_R, n_{I,0}, \epsilon} \quad q(\bar{M}_{n,f} - \bar{M}_{n,d})^2 + r_1\epsilon + s_{dT_R}\Delta dT_R^2 \quad (6.1a)$$

$$\text{s.t} \quad \dot{x}(t) = f(t, x(t), u(t), \theta) \quad (6.1b)$$

$$y(t) = g(t, x(t), u(t), \theta) \quad (6.1c)$$

$$z(t) = h(t, x(t), u(t), \theta) \quad (6.1d)$$

$$t_{f,min} - \epsilon \leq t_f \leq t_{f,max} + \epsilon \quad (6.1e)$$

$$X \geq X_d \quad (6.1f)$$

$$Q_{J,d} \geq Q_{J,min} \quad (6.1g)$$

$$T_{R,min} \leq T_R \leq T_{R,max} \quad (6.1h)$$

$$dT_{R,min} \leq dT_R \leq dT_{R,max} \quad (6.1i)$$

$$n_{I,0,min} \leq n_{I,0} \leq n_{I,0,max} \quad (6.1j)$$

Here,  $T_{R,0}$  is the initial reactor temperature,  $dT_R$  is the reactor temperature derivative and  $n_{I,0}$  is the initially loaded amount of initiator. These variables are the decision variables used to obtain the minimum value of the objective function.

The objective function consists of the quadratic deviation between the final product number average molecular weight  $\bar{M}_{n,f}$  and the desired quality  $\bar{M}_{n,d}$ , the linearly weighted slack variable of the batch time constraint and a quadratic term providing change rate penalization of the temperature derivative. Quadratic weighting is chosen for the average molecular weight deviation, as a small deviation from the desired quality can be accepted, but a large deviation must be given a high penalty. For the batch time term, a special solution is used. The more common way to minimize time in optimization problems is to introduce a variable transformation for the time  $\tau = t/t_f$ , enabling to directly optimize the time as a decision variable [41]. In this case, an NMPC base formulation and an application used to run NMPC is applied to solve the problem. This application uses a specific framework where normalization of the time is impossible without making extensive changes in the framework. Instead, the batch time is constrained in a small region close to 0, and a slack variable  $\epsilon$  is added to avoid infeasibility arising from the increasing batch time. This slack variable is then weighted with a linear weight  $r_1$ , which gives a strong penalization of large time usage. The solving of the optimization problem with respect to batch time optimization is further discussed in Section 6.3. The last term, meaning the penalty of the change of  $dT_R$  between two samples is added to ensure a relatively smooth temperature trajectory, as this is preferred in operation of the reactor. The notation  $\Delta dT_R$  is chosen because it fits well into the framework of the NMPC tool, although it is not necessarily meaningful in terms of mathematical formulation.

The constraints 6.1b-6.1d represent the process model. As already mentioned, the batch time is penalized by using a “soft constraint” and a slack variable, and this constraint is given by Equation 6.1e. The batch time is defined as the time when the desired conversion  $X_d$  is reached, and constraint 6.1f ensures that this requirement is met. Constraint 6.1g states that the cooling demand must comply with the limitations on cooling capacity. To keep within the safe region of operation, the temperature is bounded by maximum and minimum bounds, and the change rate of the temperature is also bounded to ensure that physical limits on temperature change are taken into account. In addition, the total loaded amount of initiator must stay within some given bounds in order to decrease the feasible region to a reasonable one.

For the cooling capacity constraint, a temperature dependent constraint is chosen as an approximation to the real case where either the amount of cooling water or the cooling water temperature will be limiting for heat transfer. This constraint is shown in Equation 6.2. Here, the cooling jacket temperature is assumed to be constant and equal to  $T_{J,const}$ .  $K_Q$  is a heat transfer coefficient holding information about the heat transfer conditions and the limitations on these. Since heat transfer characteristics of the modeled reactor is not known in detail, this coefficient is chosen in a way such that the constraint 6.1g clearly limits the possible choices for optimal reactor temperatures. Hence,  $K_Q$  is set to a value that gives active cooling capacity constraint in parts of the batch process.

$$Q_{J,min} = K_Q(T_{J,const} - T_R) \quad (6.2)$$

The values of the bounds and other parameters used in the formulation are given in Table 6.1. In order to obtain an easily scaled system, the loaded amount of monomer is set to 1 mole. This influences the choice of the upper bound on the initiator amount.

**Table 6.1:** Values of the parameters in the optimization problem.

<b>Description</b>	<b>Symbol</b>	<b>Value</b>
Desired number average molecular weight	$\bar{M}_{n,d}$	100.0 kg/mol
Lower bound on batch time	$t_{f,min}$	0 min
Upper bound on batch time	$t_{f,max}$	0.1 min
Desired conversion	$X_d$	0.8
Empirically determined heat transfer coefficient	$K_Q$	0.1 W/K
Constant cooling water temperature	$T_{J,const}$	10 °C
Lower bound on temperature	$T_{R,min}$	100 °C
Upper bound on temperature	$T_{R,max}$	140 °C
Lower bound on temperature derivative	$dT_{R,min}$	-0.5 K/s
Upper bound on temperature derivative	$dT_{R,max}$	0.5 K/s
Lower bound on total initiator loaded	$n_{I,0,min}$	0.00 mol
Upper bound on total initiator loaded	$n_{I,0,max}$	0.01 mol

### 6.3 Solving the Optimization Problem

The optimization problem is solved using Cybernetica CENIT, which is an application for NMPC and integrated process estimation (states and parameters). It is for online use, and communicates with the plant through an OPC (open platform communication) server. The same framework can be used to run the application offline, and in this case, the OPC server communicates with Cybernetica RealSim, which simulates an instance of the model as if it was the real plant.

In CENIT, the dynamic optimization problem shown in Section 2.6 is solved using an SQP algorithm. The structure of this general dynamic optimization problem can be adapted to almost any specialized dynamic optimization problem, such as the one given in Equation 6.1. In the NMPC application, this optimization problem is solved at every time instant, but for an offline optimization routine it is only necessary to run the optimization algorithm initially to obtain the predicted states and inputs for the entire batch. Therefore, it is important to choose the prediction horizon sufficiently long to ensure that the batch finalizes within the given time frame. The prediction horizon used in solving the optimization problem 6.1 is set to 4 hours.

As mentioned in Section 2.5, the SQP algorithm is formulated in a way that ensures convergence at infinitely many iterations. However, for the optimization to be efficient in terms of the computational effort associated with solving it, a limited number of SQP iterations must be set. In the case of applying NMPC to a system, complete convergence to the optimal solution is not necessarily needed, as it is only required that the system moves towards the desired state from sample to sample. However, in offline optimization, where the goal is to achieve an optimal solution in one run of the SQP algorithm, complete convergence is required. In this case, the limitation of the number of SQP iterations is set to 20.

The time associated with finalizing the batch and the desired product quality poses a trade-off problem. High temperatures and large amounts of initiator will hike the conversion rate and therefore shorten the batch time, but at the expense of a low  $\bar{M}_{n,f}$ . This means that an acceptable deviation from the product quality at the end of the batch will have to be defined, and for the purpose of this study it is attempted is to keep  $\bar{M}_{n,f}$  within  $\pm 1.0$  of the desired number average molecular weight of  $100.0 \text{ kg/mol}$ .

For the purpose of the optimization, the batch time is added to the state vector of the model, and this state variable is copied into an output variable. This variable is simply a counter that adds each sample to the total time and converts it from seconds to minutes.

In order to be able to optimize the initial temperature, either for isothermal optimization or for optimization of a temperature profile, an input variable  $T_{R,0}$  is added to the input vector. The optimal initialization of the temperature is implemented using this variable as a decision variable in the first sample of the prediction horizon. An internal logical variable in the model then ensures that this decision variable is replaced by  $dT_R$  for the remaining samples in the prediction horizon. Optimal initialization of the initiator amount is also required, and here, another approach is used. An extra input variable  $n_{I,0}$  representing the optimal total initiator amount is made. In addition, a state variable  $n_{I, fed}$ , keeping track of the amount of initiator that has been fed to the reactor, is created. Then, the change rate of the initiator is calculated as:

$$\frac{dn_I}{dt} = R_I V + \frac{(n_{I,0} - n_{I, fed})}{\tau_I} \quad (6.3)$$

If the time constant  $\tau_I$  is chosen sufficiently small, the system will act as if the initiator was initially loaded into the reactor. In this case, the time constant is set to 60 seconds.

To replicate real operation where the product is removed or further processed once the batch is ready, all time derivatives are set to zero in the point where 80% conversion is reached. It is desired to weight the average molecular weight deviation and the batch time in the exact point when the batch is finalized, which is an unknown point prior to optimization. Including this logic opens for weighting these variables in the last point of the prediction horizon, because all variables will hold the same value at 80% conversion and in the end of the prediction horizon. However, the same logic could be problematic for the numerical properties of the problem, especially with the long sampling time of 15 seconds. The batch can reach 80% conversion at any point, also between two samples. However, the derivatives will be set to zero from the next sample, regardless of where the exact 80% mark occurs. This is illustrated with the solid line in Figure 6.2. The solver in CENIT makes perturbations in the input variables to determine the sensitivity in the output variables, as an alternative to calculating derivatives. If the perturbations are too small to move the 80% mark before the current sample or after the next sample, the sensitivity of the batch time variable will be set to zero for some or all of the input variables. To avoid this, linear interpolation can be implemented to circumvent the

problem by setting the derivatives to zero in the exact point where 80% conversion is reached. The dashed line in Figure 6.2 illustrates the resulting conversion with linear interpolation.

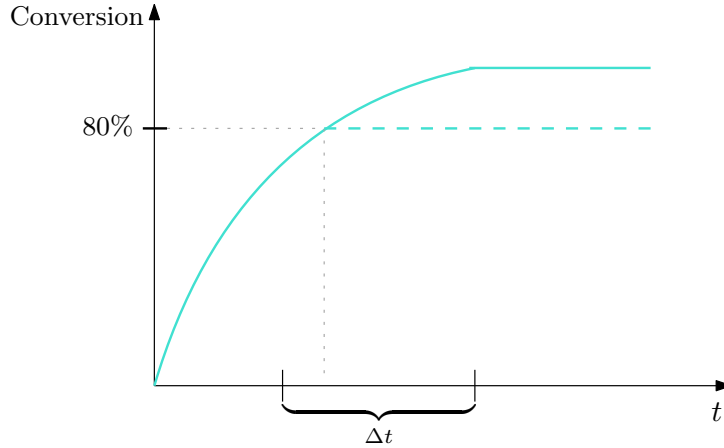


**Figure 6.2:** Conversion as a function of time with (dashed line) and without (solid line) interpolation.

The linear interpolation is implemented by using relational and logical operators to determine if the conversion will reach 80% between the current sample and the next. If that is the case, all derivatives are scaled by a factor  $\frac{\Delta\tau}{\Delta t_{int}}$ .  $\Delta\tau$  is the time from the current sample mark to the time where 80% conversion is reached, calculated using the expression shown in Equation 6.4.

$$\Delta\tau = \frac{(0.8 - X_k)\Delta t_{int}}{X_{k+1} - X_k} \quad (6.4)$$

Here,  $X_k$  and  $X_{k+1}$  are the conversions at the current and the next sample, respectively.

To reduce the number of decision variables arising from the optimization of the temperature profile, the input blocking part of the NMPC formulation is utilized. The prediction horizon of 240 minutes with sample intervals of 15 seconds is divided into 185 blocks for the temperature derivative input variable  $dT_R$ . This gives only 186 decision variables to calculate for the temperature profile (including initial temperature), compared to 961 variables without input blocking. The blocking structure is finer at the beginning of the prediction horizon giving the temperature freedom to vary in this region, and the resolution is decreasing throughout the prediction horizon. A new temperature derivative is calculated every sample for the 50 first samples. Then, the manipulated variable is allowed to change every fifth sample until sample 725 (181.25 minutes), where a single block is used for the rest of the prediction horizon. At this point, the batch is expected to be close to finished, and the choice of temperature in this region does not affect the polymer product.

## 6.4 Results and Discussion

In this section, results from relevant simulations and optimization of the model are given. The optimization procedure is developed through three steps. First, only the optimal monomer to initiator ratio is calculated for a given constant temperature ( $u = n_{I,0}$ ). Further, an optimal constant temperature is added to the formulation ( $u = n_{I,0}, T_{R,0}$ ), and finally, both the monomer to initiator ratio and the dynamic temperature trajectory are optimized in order to produce the shortest possible batch time ( $u = n_{I,0}, T_{R,0}, dT_R$ ).

The various weights applied in the optimization problem in the different steps of optimization are obtained by tuning the problem using a trial and error methodology. The starting point for this tuning is an educated guess on what would be a good combination of weights, given the objective at hand. The importance of attaining the correct quality and a short batch duration is apparent, compared other variables in the problem. However, tuning the optimization routine has shown to be a time consuming task.

The model is used with parameters from literature, given in Appendix A, not the estimated parameters from Section 5.1, for all optimization calculations. This is mainly because the fitted model does not show improvement in predicting the final product quality, which is of interest in the case of optimization. In addition, the lack of basic data to support the calculated parameter changes makes it hard to conclude that the fitted model better represents the real process, compared to the model parameters supported by experimental results.

### 6.4.1 Pre-Optimization Simulation

Pre-optimization simulations were performed to get an overview of how the model reacts to changes in the input variables, to generate a base case for comparison, as well as indicating an optimal region of process conditions. The model is simulated for constant temperatures in the range of 100 to 140 °C and for monomer to initiator ratios between 20 and 200. The simulation is terminated when the conversion has reached 80%, which is defined as the end of the batch, and the number average molecular weight is stored in this point.

The resulting number average molecular weights as a function of the input variables are shown in the surface plot in Figure 6.3. The black line in the plot shows the intersection between the surface and the plane  $\bar{M}_n = 100.0 \text{ kg/mol}$ .

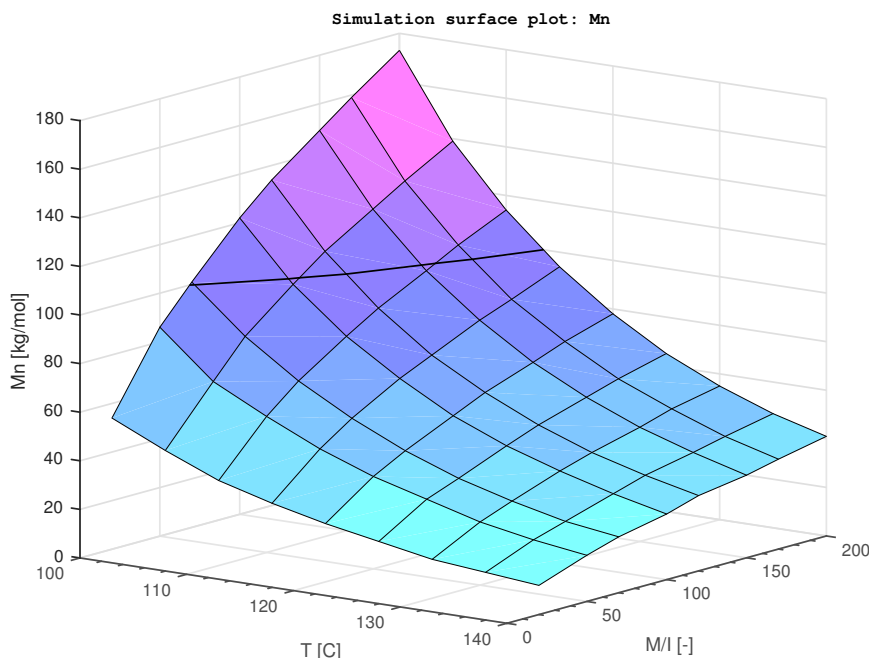


**Figure 6.3:** Surface plot of  $\bar{M}_n$  as a function of isothermal temperature and monomer to initiator ratio.

Equivalent simulation results for the batch time are shown in Figure 6.4. Similarly as for the number average molecular weight landscape plot, the black contour curve represents the process conditions that give the desired product quality.

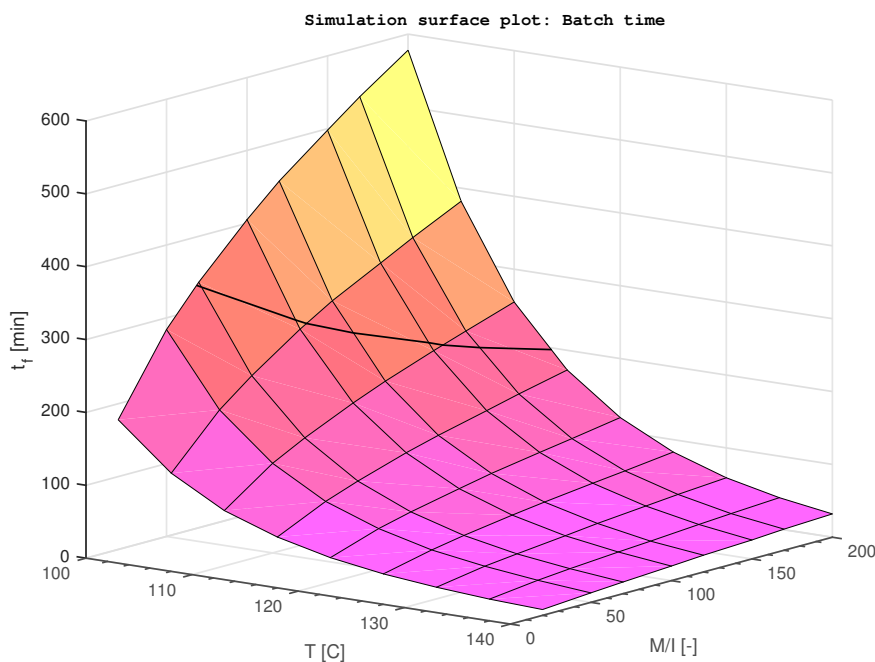


**Figure 6.4:** Surface plot of batch time as a function of isothermal temperature and monomer to initiator ratio.

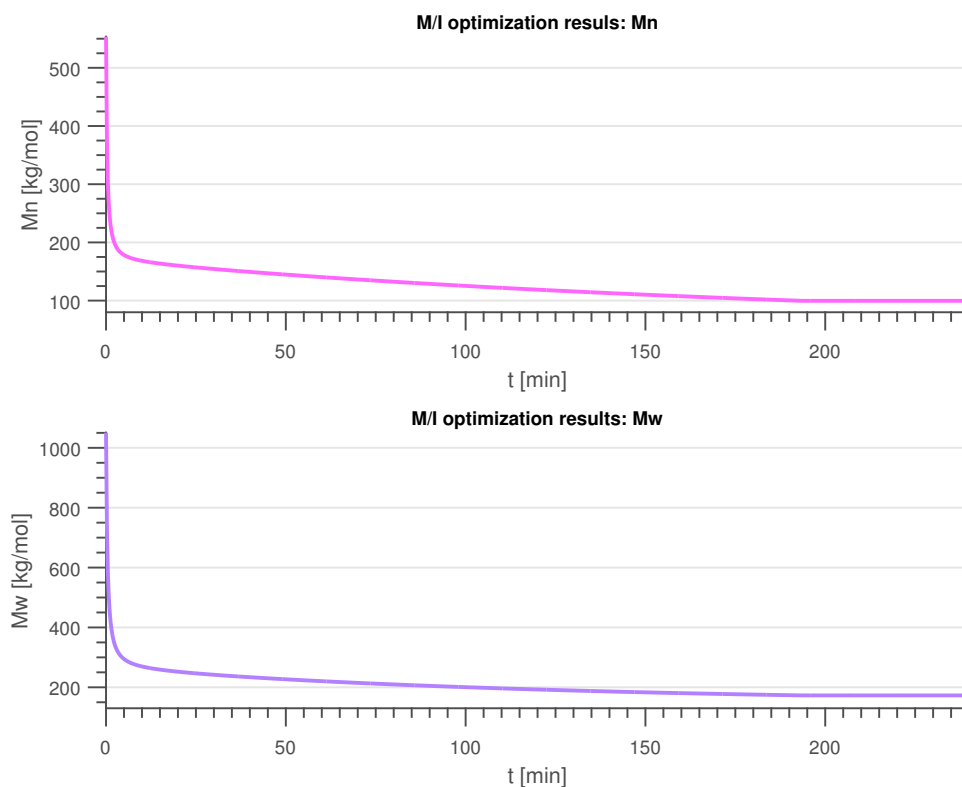
As expected, the number average molecular weight is decreasing with increasing temperatures and initiator amounts (at low monomer to initiator ratios). Higher temperatures activate the initiation reaction. As a result, monomer molecule consumption is spread over many chains, giving a high number of shorter chains compared to lower temperature conditions. The same principle applies to large amounts of initiator in the system, as many radical chains will exist at the same time in such conditions. The intersection of the desired  $\bar{M}_n$  plane shows that according to the model, it is only possible to produce the desired product quality at constant temperatures below 120 °C, as higher temperatures will always give a lower molecular weight. The range of possible initiator contents is slightly wider than the temperature range, and amounts between 0.0143 and 0.005 mol of initiator per mol styrene can be added to the reactor to produce the desired quality.

The batch time follows the same trend as the molecular weight. Producing higher number average molecular weights requires more time - up to 10 hours. In comparison, the time associated with polymerization of the shortest chain lengths is only a few minutes. The time it takes to produce  $\bar{M}_n = 100.0 \text{ kg/mol}$  is between 337 and 198 minutes for the different reactor conditions. This means that the optimal point in this case is the point where the batch time equals 198 minutes. In this point, the constant reactor temperature is 113.5 °C and the mole based ratio between monomer and initiator is 200.

## 6.4.2 Optimization of Monomer to Initiator Ratio

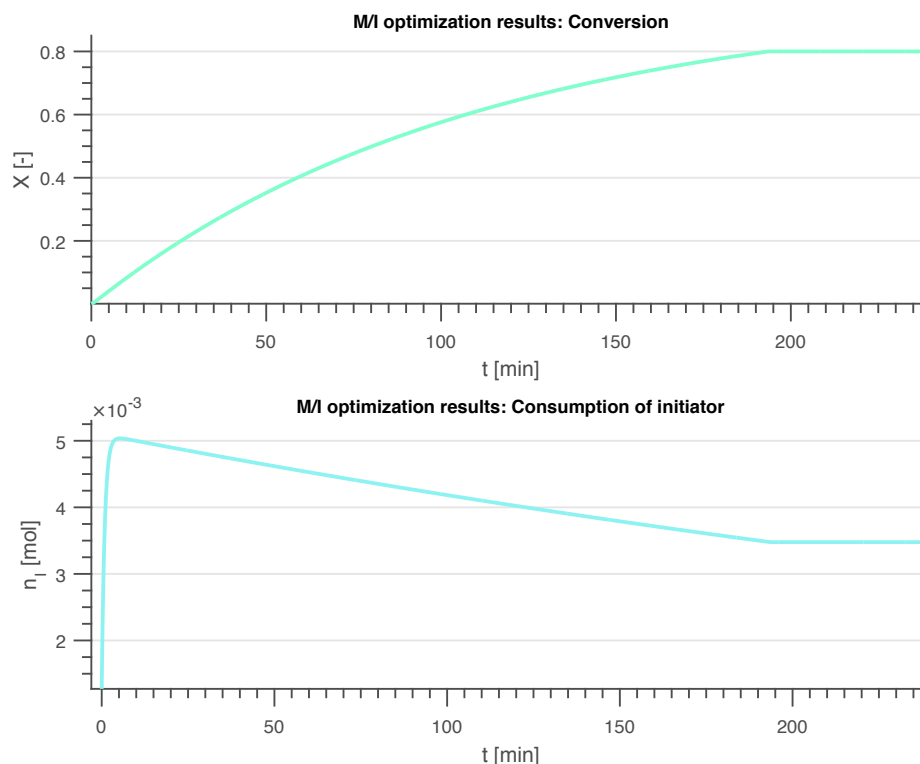
In this part, only the monomer to initiator ratio is optimized. The reactor temperature is set to a constant value of 113.5 °C, from the optimal point in the pre-optimization simulations. In the optimization formulation, all relevant variables are scaled with their expected maximum value. The deviation from the desired product quality is weighted with  $q = 450$ , and the batch time constraint violation is weighted with  $r_1 = 0.01$ . The product quality weight is significantly larger than the slack variable weight for the batch time for two reasons. First, the product quality is weighted in only one point, compared to the batch time which is weighted at every point in the prediction horizon. The total penalization is the sum of the penalizations in every time step. Secondly, the batch time constraint is linearly weighted, which means that the penalization is high for every deviation from the constraints. For the batch time, this deviation will grow larger for each time step.

Figure 6.5 shows the development of the number and weight average molecular weights. In the beginning, the average molecular weights take high values, and they stabilize at a much lower level throughout the batch. This development is due to that only a few initiator molecules have decomposed to activate new chains in the first few minutes, and propagation is rapid on these chains due to the high monomer concentration. The number average molecular weight is 99.6 kg/mol at the time when 80% conversion is reached, which is well within 1% deviation from the desired value. The corresponding value for  $\bar{M}_w$  is 172.9 kg/mol, meaning that the polydispersity index is equal to 1.74. This PDI is within the expected range which is between 1.5 and 2.0 for polymers produced by a free-radical production mechanism [42].



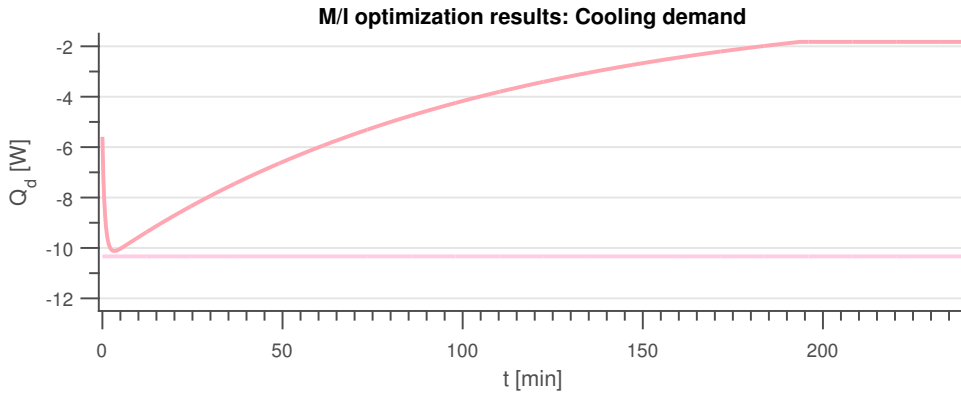
**Figure 6.5:** Number and weight average molecular weights for monomer to initiator ratio optimization at 113.5 °C.

Figure 6.6 gives the dynamic styrene conversion and the initiator consumption for the calculated monomer to initiator ratio. The monomer conversion follows a smooth path to the 80% conversion mark where the batch is finalized. The optimized monomer to initiator ratio is 196.4, corresponding to an initiator amount of 0.0051 mol of initiator per mol of styrene. The optimal amount of initiator calculated is added to the reactor during the first minutes, as can be seen from the steep increase in the initiator content. It should be noted that this delay can cause some inaccuracy in the calculated batch time, making it longer than the true value. The initiator content in the reactor settles at 0.0035 mol, which is a reduction of only 31% from the total added amount. This suggests that having a high accessibility of initiator molecules in the beginning of the batch reduces the batch time, as expected. However, there will be small amounts of residual initiator in the final product.



**Figure 6.6:** Monomer conversion and initiator consumption for monomer to initiator ratio optimization at 113.5 °C.

The cooling demand needed to keep the temperature constant at 113.5 °C is shown in Figure 6.7, along with the linear cooling constraint corresponding to Equation 6.2. The cooling constraint is never active, but the cooling demand comes relatively close to the constraint at one point a few minutes from the onset of the reaction. This means that it is in this case not required to use the entire cooling capacity to maintain the calculated optimal temperature, even in the point of maximum heat generated by the reaction.



**Figure 6.7:** Cooling demand and cooling capacity constraint for monomer to initiator ratio optimization at 113.5 °C.

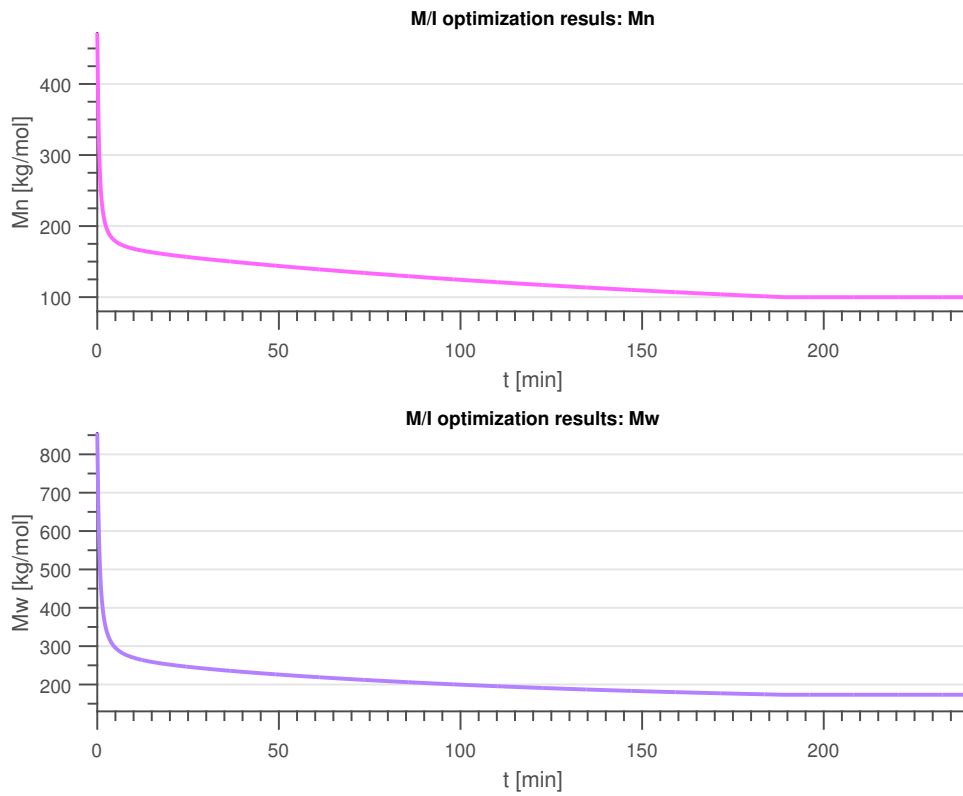
In this case, the SQP algorithm converges in 6 iterations. As can be seen from the figures above at the point where all derivatives are set to zero, the resulting batch time is 194.1 minutes.

The polymerization time is 3.9 minutes shorter compared to the optimal pre-optimization simulation results. This improvement in batch time is assumed to arise from the increased amount of initiator present in the system. By allowing a tiny negative deviation from the exact desired quality value, a small increment in the initiator amount can be added, resulting in a slightly shorter batch time. However, looking at the results from a wider perspective, it can be said that the calculated monomer to initiator ratio is a replicate of the optimal point seen in the pre-optimization calculations. This discovery supports the optimization formulation’s ability to find the true minimum in the feasible region.

### 6.4.3 Optimization of Monomer to Initiator Ratio and Constant Temperature

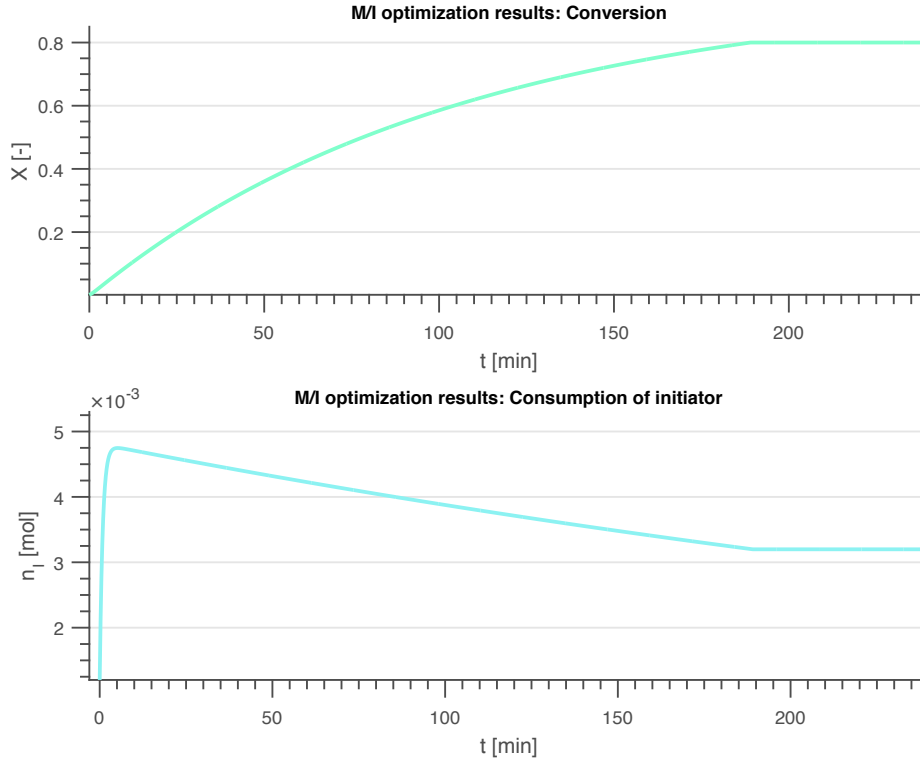
As a natural development from only optimizing the initiator content, both the monomer to initiator ratio and the constant temperature  $T_{R,0}$  are optimized. The weights used in the optimization problem formulation are the same as the ones given in the previous section, and the variables are scaled in the same way.

The resulting number and average molecular weights throughout the batch are shown in Figure 6.8. The development of these are similar to the result seen in Figure 6.5. The final number average molecular weight  $\bar{M}_{n,f}$  of 100.0 kg/mol is exactly on the target value of  $\bar{M}_{n,d}$ . This result shows that enabling fine tuning of the constant temperature, in addition to optimizing the monomer to initiator ratio, improves the quality towards the desired value. The final weight average molecular is 173.3 kg/mol, which gives a polydispersity index of 1.73.



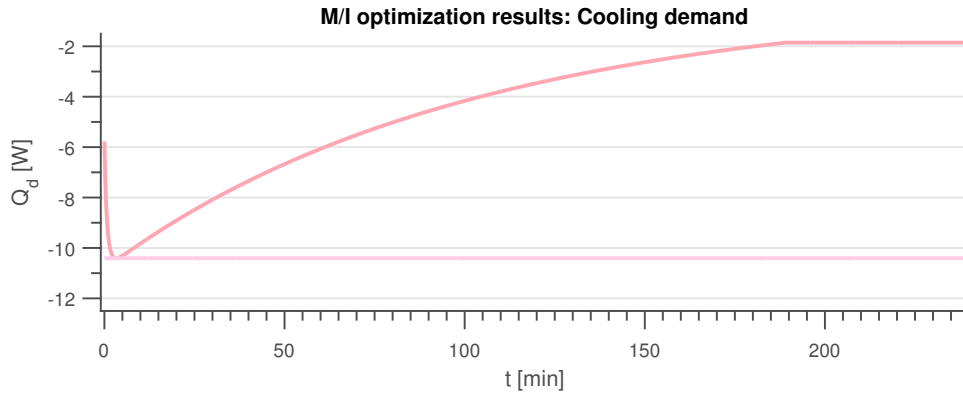
**Figure 6.8:** Number and weight average molecular weights for monomer to initiator ratio and constant temperature optimization.

Figure 6.9 gives the dynamic conversion and initiator reactor contents. The optimal monomer to initiator ratio calculated in this case is 208.2, meaning that 0.0048 mol of initiator is added to the system. Also in this case, only a small portion of the available initiator is consumed in the process, leaving a relatively large residual amount, compared to the charged initiator amount.



**Figure 6.9:** Monomer conversion and initiator consumption for monomer to initiator ratio and constant temperature optimization.

The optimal constant temperature  $T_{R,0}$  is calculated to be  $114.2^{\circ}\text{C}$ , which is fairly close to the minimum time temperature identified in the pre-optimization simulations. The cooling duty required to keep the temperature constant at this value, given the heat generation from the polymerization reactions, is given in Figure 6.10. The linear constraint from Equation 6.2 is also shown in the figure. In the point of maximum reaction heat generation, the cooling capacity constraint is active. Since the optimal reactor conditions in this case is quite similar to those of the optimization in Section 6.4.2 where the constraint is not active, it is not expected that relaxing this constraint would give a significantly improved solution in terms of batch time. However, the relation between initiator concentration, temperature and cooling demand is rather complex. Choosing a higher constant reactor temperature gives an increased propagation rate, which will further result in enlargement of the heat of reaction. The higher reactor temperature will give a decline in cooling demand, while the increased heat generation will simultaneously increase the need of cooling. Similarly, a change in initiator concentration will also influence the propagation rate due to the dependence of radical chain concentration, altering the demand for cooling.



**Figure 6.10:** Cooling demand and cooling capacity constraint for monomer to initiator ratio and constant temperature optimization

The SQP algorithm converges for the given decision variables in 8 iterations. The resulting batch time is 189.5 minutes, which is 8.5 and 4.6 minutes shorter than the pre-optimization simulation solution and the monomer to initiator ratio optimization at  $T_R = 113.5^\circ\text{C}$ , respectively. The optimal initiator addition is here slightly lower than both the previous cases, and the corresponding constant temperature is slightly higher. The higher temperature allows for faster polymerization, which gives the improvement in the end time of the batch, and less initiator is optimal in order to keep  $\bar{M}_n$  sufficiently high given the increased temperature.

#### 6.4.4 Optimization of Monomer to Initiator Ratio and Temperature Profile

As a final step in the process towards finding a complete set of optimal reactor conditions according to the scope of this work, the reactor temperature is allowed to vary in time, including  $dT_R$  as a manipulated variable along with the initial temperature and the initiator amount. The weights used in the optimization problem are shown in Table 6.2.

**Table 6.2:** Weights in the optimization of monomer to initiator ratio and reactor temperature trajectory.

Weight	Value
$q$	450.0
$r_1$	0.01
$s_{dT_R}$	1.0

The product quality weight and the batch time constraint weights are the same as in the previous cases.  $s_{dT_R}$  is set to 1.0 by trial and error, as this part of the problem formulation must be perfectly tuned to obtain the correct behavior. It is desired to penalize the change rate of the temperature derivative in order to obtain a smooth temperature profile without oscillations, that can easily be implemented as an optimal path for a real process application. On the other hand, this variable must be given sufficient freedom to move in order to produce a temperature profile that gives optimal performance.

The resulting number and weight average molecular weight developments are shown in Figure 6.11. The development is similar to the ones seen for constant temperature operation, only different in the approximately linear decline with respect to time after the initial region of high average molecular weights. The end number average molecular weight is  $99.9\text{ kg/mol}$ , which

is only 0.1% from the desired value. This shows that including more degrees of freedom in the problem allows for increased precision when it comes to end product quality. However, the measurement uncertainty for molecular weight measurements is expected to be multiple times this model precision, and it can therefore improbably be fully exploited in a real process application. The weight average molecular weight is 182.9 kg/mol, giving a polydispersity index of 1.83. This value of the PDI is about 0.1 units higher than seen for the constant temperature cases, meaning that having varying temperature in this case results in a wider molecular weight distribution.

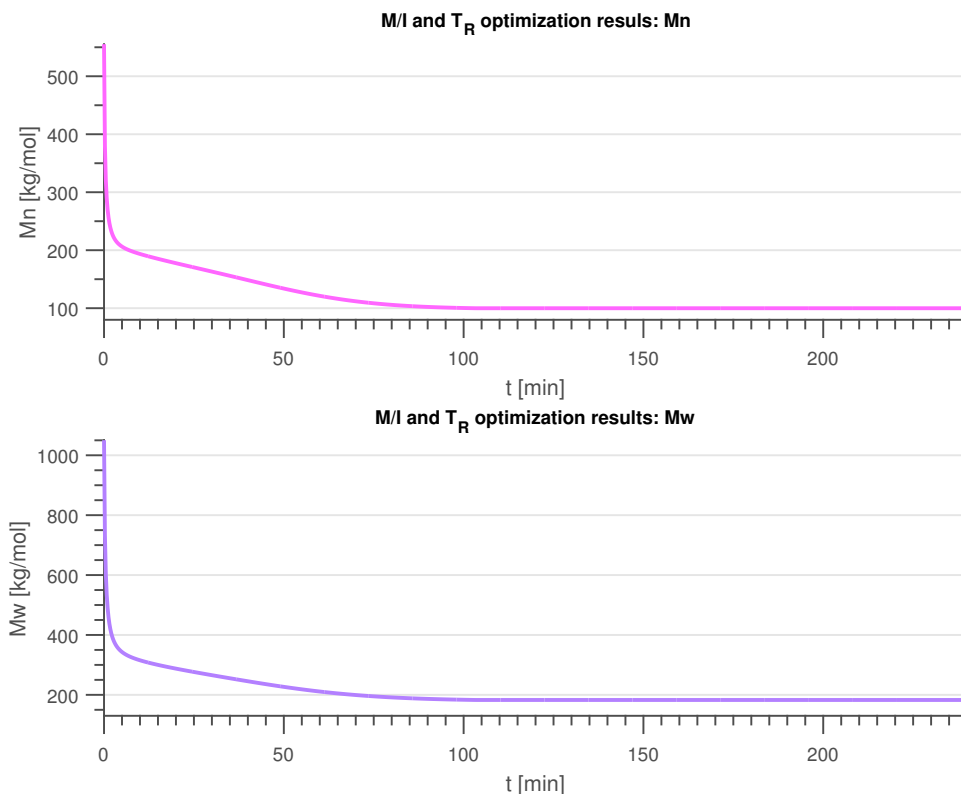


**Figure 6.11:** Number and weight average molecular weights for monomer to initiator ratio and temperature profile optimization.

The styrene conversion and initiator content development are shown in Figure 6.12. The conversion rate in the beginning of the batch is significantly larger than the conversion rate of the optimal cases with constant temperature shown in Figures 6.6 and 6.9. The monomer to initiator ratio calculated in this case is 647.9, meaning that the optimal initiator amount is very small and equal to 0.0015 mol. Because the temperature trajectory shown in Figure 6.13 is in a significantly higher range than the constant temperatures calculated in the previous sections, it is necessary to reduce the initiator concentration in order to keep the number average molecular weight at a sufficiently high level to meet the quality requirements at the end of the batch. However, it is important to note that ability to dose such a small portion of initiator with high precision is highly unlikely in a practical application. In addition, the model assumes an ideal case where no initiator is lost to the continuous phase, which will not be entirely true in a real process.

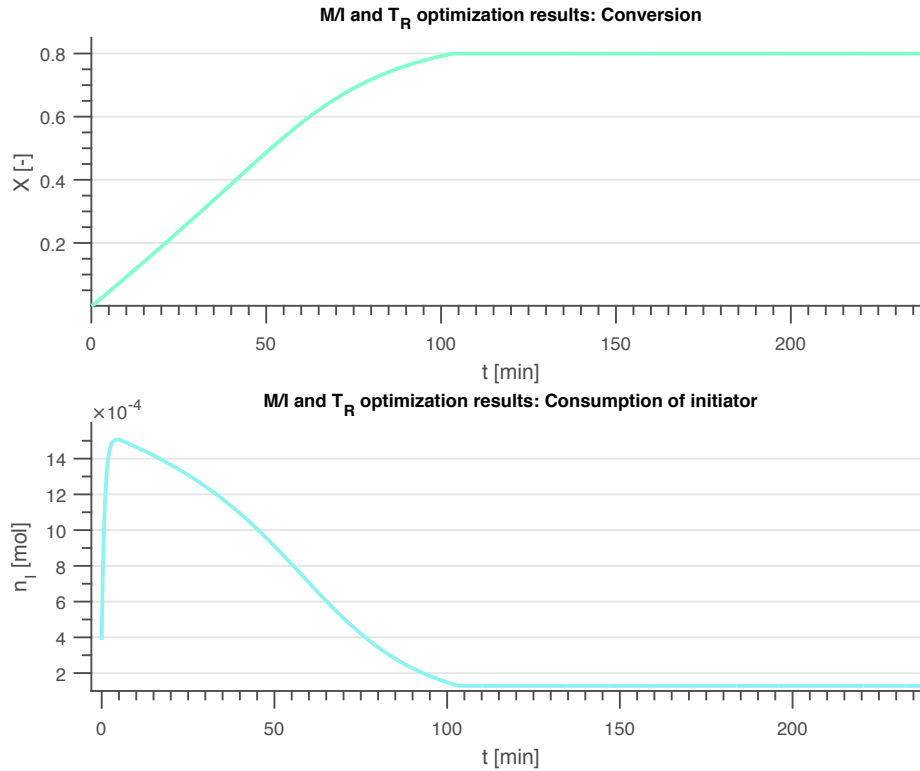


**Figure 6.12:** Styrene conversion and initiator consumption for monomer to initiator ratio and temperature profile optimization.

Finally, the optimal temperature profile and the cooling demand with the temperature difference dependent cooling constraint are shown in Figure 6.13. The optimal initial temperature  $T_{R,0}$  is calculated to be 121.7 °C. From the initial point, the temperature increases slowly to the maximum allowed temperature of 140 °C during the first 85 minutes of the batch. The cooling constraint reflects the changes in the reactor temperature according to Equation 6.2, and the constraint is active in the time period from 5 minutes to 40 minutes into the batch. This means that the allowed temperature in this region is constrained by the available heat transport to the cooling system. Because of the relatively large time period of active cooling capacity constraint, it is likely that this constraint affects the quality of the optimization solution. Without this constraint present, the optimization routine could possibly find another temperature path that gives improved batch time.

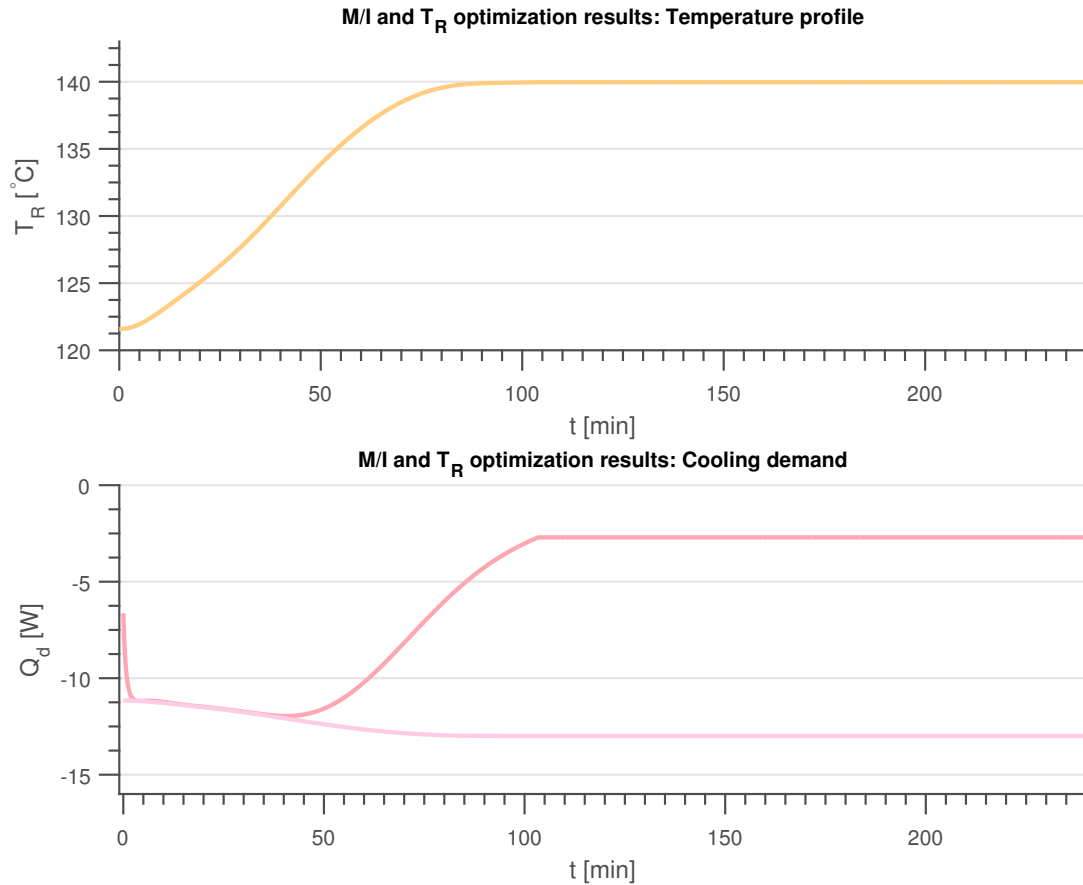


**Figure 6.13:** Temperature profile and cooling demand for monomer to initiator ratio and temperature profile optimization.

In this case, the SQP algorithm converges in 5 iterations, and the resulting batch time is 103.9 minutes. This is 94.1, 90.2 and 85.6 minutes shorter than the pre-optimization simulation, the isothermal monomer to initiator ratio optimization and the combined temperature and monomer to initiator ratio optimization for isothermal operation, respectively. This means that allowing the temperature to vary, using an optimal temperature trajectory compared to optimal isothermal operation is gives a significant reduction of the batch duration.

The above results are obtained with a constant cooling water temperature of 10 °C. As mentioned in the introduction of Section 6, the cooling water temperature often varies throughout the year. Corresponding results as the ones shown in this section, using a cooling water temperature of 20 °C are shown in Appendix B. The temperature profile and cooling demands of the two cases are compared in Figure 6.14.

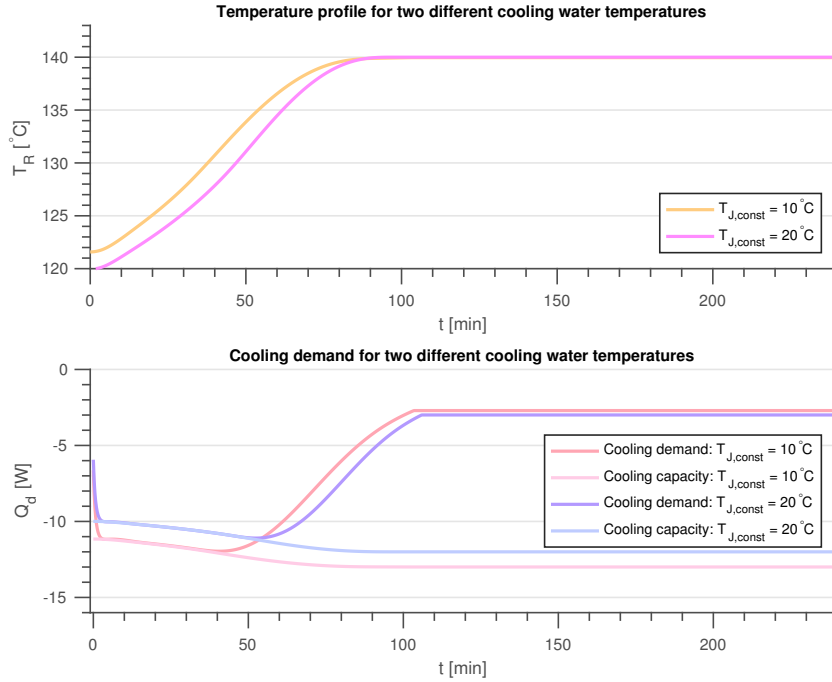


**Figure 6.14:** Temperature profile and cooling demand for cooling water temperatures of 10 and 20 °C.

Using a higher cooling water temperature gives a tighter bound on the cooling demand. This causes a small reduction in quality performance and the batch time is slightly increased. The temperature profile starts at a lower value, and it stays below the temperatures of the original case. However, the temperature reaches the maximum limit approximately at the same point in time. In addition, the initiator amount is a bit higher. This means that there exist optimal actions to handle the changed cooling capacity and mitigate the effects on product quality and polymerization time. The conclusion is that utilizing updated information on the available cooling resources is important to make the correct decisions on what recipe to use and what temperature setpoints the reactor should be controlled to.

### 6.4.5 Summary

Table 6.3 shows a summary of the attained optimization results.

**Table 6.3:** Key numbers from the optimization results.

Case	Decision variables	$T_R$ [°C]	$M/I$ [-]	$t_f$ [min]	$M_{n,f}$ [kg/s]	# SQP iterations
Isothermal, simulation	–	113.5	200	198.0	100.0	–
Isothermal, optimal $M/I$	$n_{I,0}$	113.5	196.4	194.1	99.6	6
Isothermal, optimal $M/I$ and $T_{R,0}$	$n_{I,0}, T_{R,0}$	114.2	208.2	189.5	100.0	8
Optimal $M/I$ and $T_R$ ( $T_{J,const} = 10^\circ\text{C}$ )	$n_{I,0}, T_{R,0}, dT_R$	121.7-140.0	647.9	103.9	99.9	5
Optimal $M/I$ and $T_R$ ( $T_{J,const} = 20^\circ\text{C}$ )	$n_{I,0}, T_{R,0}, dT_R$	121.0-140.0	625.0	106.4	99.8	6

Overall, the observed trend shows that allowing more variables to be determined by the optimization routine, the initiator amount is reduced and the temperature increased to produce the correct number average molecular weight in the least amount of time. It is also apparent that increasing the number of optimized variables, the duration of the batch is shortened while

the product quality precision remains high. This is especially seen in the last case where the monomer to initiator ratio and the temperature trajectory in time are optimized. As mentioned in Section 6.3, this case has a total of 187 decision variables, compared to 1 and 2 in the isothermal optimization cases with given and optimized temperature, respectively. The increased freedom to optimally determine temperature dynamically shows a powerful effect in the end time of the batch. The number of SQP iterations does not seem to be systematically affected by the change in the decision variable set, but the time associated with one SQP iteration increases significantly when introducing time varying temperature.

## 7 Conclusion

Theoretical concepts regarding modeling of polymerization processes and semi-batch reactors have been established in this report. This gave a basis for the development of a model from first principles. The result was a simple and numerically robust model, enabling for application of a simple solver, which provided for low computational effort in simulation. It was also qualitatively in accordance with expectations with respect to how it reacts to changes in initiator and blowing agent concentrations, as well as reactor temperature.

Parameters collected from experimental research literature were applied to the model, and an attempt of improving these parameters in order to restore a very limited set of measurements from a lab-scale plant was performed. Unfortunately, lack of high quality basic data is a key issue in the polymer industry, as measurements of many important variables have slow dynamics and are associated with high uncertainty. The result from the performed parameter estimation showed improved dynamic characteristics but the precision in predicting the end product quality was seemingly not enhanced. It is therefore recommended to perform further work with the model in the line of parameter estimation and model validation with access to extended supporting data that covers the entire duration of the batch. A good fit between the model and the real process is crucial to have in place before the model is applied to a real system for offline optimization, NMPC or DRTO.

Overall, the results from the optimization part of this work proved that increasing the number of degrees of freedom available for optimization reduced the time associated with producing the desired end product quality at 80% conversion. Moreover, choosing higher temperatures in order to improve the batch time, and at the same time reducing the initiator concentration to keep the number average molecular weight at the high desired level of  $100.0 \pm 1.0$  kg/s, appeared to be optimal. The optimization routine was in all the investigated cases able to produce this desired product quality with high precision. However, the measurement uncertainty associated with molecular weight measurements is often high, and therefore, it is doubtful that the full potential of this precision can be exploited in a real process application.

Optimization of the monomer to initiator ratio and the temperature trajectory turned out to give very promising results. Using optimally varying temperature was according to the model capable of reducing the batch duration with 1.5 hours, compared to optimal isothermal operation. Because the model used was not properly fitted to the real process, and several rough assumptions were made in the development of the model, these results can only be said to be qualitatively correct. However, the conclusion is that allowing the temperature to optimally vary in contrast to isothermal operation could potentially give significant improvements in plant capacity utilization for EPS production facilities.

Investigations on optimal conditions with two different cooling water temperatures were also performed. The results proved that there exist optimal actions to mitigate the effects on the end product quality and batch duration with disturbances in the cooling water temperature. In conclusion, it is useful to re-optimize once new information about the availability of resources comes to light. Preferably, the combination of NMPC and DRTO, which re-optimizes for disturbances while the batch process is operating and tracks the path changes, should be applied to the system. This is a natural next step in the future work with this system.

## References

- [1] B. Foss and T. A. N. Heirung, “Merging optimization and control.”
- [2] PlasticsEurope, “Expanded polystyrene.” <http://www.plasticseurope.org/what-is-plastic/types-of-plastics-11148/expanded-polystyrene.aspx>.
- [3] S. Tørgersen, “Expandable polystyrene: a case study for low cost manufacturing.” <http://www.averis.no/?p=458>.
- [4] T. S. Schei, “On-line estimation for process control and optimization applications,” *8th International IFAC Symposium on Dynamics and Control of Process Systems*, vol. 2, 2007.
- [5] M. A. Hosen, M. A. Hussain, A. Khosravi, D. Creighton, and S. Nahavandi, “Investigation of process dynamics and control of polystyrene batch reactor using hybrid model,” in *WCECS 2012: Proceedings of the World Congress on Engineering and Computer Science*, pp. 765–769, Newswood Limited, 2012.
- [6] J. Bausa, “Model based operation of polymer processes, what has to be done?,” *Macromolecular Symposia*, vol. 259, no. 1, pp. 42–52, 2007.
- [7] A. Kumar and R. K. Gupta, *Fundamentals of Polymer Engineering. Second Edition. Revised and Expanded*. 2003.
- [8] C. Kiparissides, “Chemical reaction engineering: From fundamentals to commercial plants and products polymerization reactor modeling: A review of recent developments and future directions,” *Chemical Engineering Science*, vol. 51, no. 10, pp. 1637 – 1659, 1996.
- [9] J. Gao, K. Hungenberg, and A. Penlidis, “Process modelling and optimization of styrene polymerization,” in *Macromolecular Symposia*, vol. 206, pp. 509–522, Wiley Online Library, 2004.
- [10] R. Machado, J. Pinto, P. Araujo, and A. Bolzan, “Mathematical modeling of polystyrene particle size distribution produced by suspension polymerization,” *Brazilian Journal of Chemical Engineering*, vol. 17, pp. 395 – 407, 12 2000.
- [11] R. Dhib, J. Gao, and A. Penlidis, “Simulation of free radical bulk/solution homopolymerization using mono- and bi-functional initiators,” *Polymer Reaction Engineering*, vol. 8, no. 4, pp. 299–464, 2000.
- [12] Polymer Properties Database, “Glass transition temperature.” <http://polymerdatabase.com/polymer%20physics/GlassTransition.html>, 2016.
- [13] A. Nyström, “Modeling and simulation of a multi phase semi-batch reactor,” 2007.
- [14] H. S. Fogler, *Elements of Chemical Reaction Engineering*. 2006.
- [15] F. Gjertsen, “Models for on-line control of batch polymerization processes,” 2013.
- [16] E. Mastan and S. Zhu, “Method of moments: A versatile tool for deterministic modeling of polymerization kinetics,” *European Polymer Journal*, vol. 68, pp. 139 – 160, 2015.
- [17] M. Rogosic, H. Mencer, and Z. Gomzi, “Polydispersity index and molecular weight distributions of polymers,” *European Polymer Journal*, vol. 32, no. 11, pp. 1337 – 1344, 1996.
- [18] J. M. Zielinski and J. L. Duda, “Predicting polymer/solvent diffusion coefficients using free-volume theory,” *AIChE Journal*, vol. 38, no. 3, pp. 405–415, 1992.

- [19] H. A. Preisig, “The ABC of Modelling.” [https://dl.dropboxusercontent.com/u/19261469/ABC\\_script.pdf](https://dl.dropboxusercontent.com/u/19261469/ABC_script.pdf).
- [20] R. Haber and L. Keviczky, *Nonlinear system identification. 1. Nonlinear system parameter identification*. Mathematical Modelling, Kluwer Academic Publishers, 1999.
- [21] H.-P. Halvorsen, “Kalmanfilter lecture notes.” <http://home.hit.no/~hansha/documents/control/Documents/Lecture%20Notes/Kalmanfilter%20-%20Forelesningsnotater.pdf>.
- [22] Mathworks, “Recursive algorithms for online parameter estimation.” <http://se.mathworks.com/help/ident/ug/recursive-algorithms-for-online-estimation.html>.
- [23] Engineering and Technology History Wiki, “Rudolf E. Kalman Biography.” [http://ethw.org/Rudolf\\_E.\\_Kalman](http://ethw.org/Rudolf_E._Kalman).
- [24] J. Nocedal and S. J. Wright, *Numerical optimization*. Springer Series in Operations Research and Financial Engineering, Berlin: Springer, 2006.
- [25] J. H. Challis, “Dynamic optimization: Basics.” <http://www.personal.psu.edu/~jhc10/KINES574/Lecture9.pdf>.
- [26] Stanford University, “User’s guide to dynamic optimization.” <http://web.stanford.edu/group/econ/uploads/pmwiki/Math.DynamicOptUserGuide.pdf>.
- [27] A. R. Secchi, “Advanced process control and real-time optimization.” <http://slideplayer.com/slide/8027926/>, 2013.
- [28] L. D. Keer, P. H. V. Steenberge, M.-F. Reyniers, K.-D. Hungenberg, L. Seda, D. R. D’hooge, and G. B. Marin, “An update on the kinetics and mechanistic understanding of the industrial production of expandable polystyrene,” 2016.
- [29] A. S. Almeida, K. Wada, and A. R. Secchi, “Simulation of styrene polymerization reactors: kinetic and thermodynamic modeling,” *Brazilian Journal of Chemical Engineering*, vol. 25, pp. 337 – 349, 06 2008.
- [30] Department of Chemistry Texas A&M University, “Polystyrene at a glance.” <http://www.chem.tamu.edu/class/fyp/stone/tutorialnotefiles/polymers/styrene.htm>, 2016.
- [31] J. Migniot, “Product information and characteristics.” <http://www.styrenemonomer.org/2.2.html>, 2012.
- [32] M. T. García, I. Gracia, G. Duque, A. de Lucas, and J. F. Rodríguez, “Study of the solubility and stability of polystyrene wastes in a dissolution recycling process,” *Waste Management*, vol. 29, no. 6, pp. 1814 – 1818, 2009.
- [33] LSU Macromolecular Studies Group, “Pentane solvent properties.” <http://macro.lsu.edu/HowTo/solvents/Pentane.htm>, 2016.
- [34] PubChem, “Physical properties of peroxides.” <https://www.ncbi.nlm.nih.gov/pccompound?term=peroxide>.
- [35] M. Frounchi, F. Farhadi, and R. P. Mohammadi, “Simulation of styrene radical polymerization batch reactor: A modified kinetic model for high conversion,” *Scientia Iranica*, vol. 9, no. 1, pp. 86–92, 2002.

- [36] G. Z. A. Wu, L. A. Denton, and R. L. Laurence, "Batch polymerization of styrene-optimal temperature histories," *Polymer Engineering & Science*, vol. 22, no. 1, pp. 1–8, 1982.
- [37] M. A. Villalobos, A. E. Hamielec, and P. E. Wood, "Bulk and suspension polymerization of styrene in the presence of n-pentane. an evaluation of monofunctional and bifunctional initiation," *Journal of Applied Polymer Science*, vol. 50, no. 2, pp. 327–343, 1993.
- [38] R. C. Gillham, "The influence of pressure on the polymerization of styrene," 1950.
- [39] E. Lehmann and G. Casella, *Theory of Point Estimation*. Springer Texts in Statistics, Springer New York, 2003.
- [40] J. Kadam, M. Schlegel, W. Marquardt, R. Tousain, D. v. Hessem, J. v.d. Berg, and O. Bosgra, "A two-level strategy of integrated dynamic optimization and control of industrial processes - a case study," *European Symposium on Computer Aided Process Engineering*, vol. 12, pp. 511–516, 2002.
- [41] O. Abel, A. Helbig, W. Marquardt, H. Zwick, and T. Daszkowski, "Productivity optimization of an industrial semi-batch polymerization reactor under safety constraints," *Journal of Process Control*, vol. 10, no. 4, pp. 351 – 362, 2000.
- [42] N. Dotson, R. Galvan, R. Laurence, and M. Tirrell, *Polymerization Process Modeling*. Advances in interfacial engineering series, Wiley, 1995.
- [43] Sigma Aldrich, "Dicumyl peroxide." <http://www.sigmaaldrich.com/catalog/product/aldrich/329541?lang=en&region=NO>.
- [44] A. W. Hui and A. E. Hamielec, "Thermal polymerization of styrene at high conversions and temperatures. an experimental study," *Journal of Applied Polymer Science*, vol. 16, no. 3, pp. 749–769, 1972.

## A Model Parameters

**Table A.1:** Values of the parameters used in the model.

Parameter	Description	Value	Unit	Source
$a$	Gel effect tuning parameter	1.75	—	[28]
$A$	Gel effect tuning parameter	0.465	—	[28]
$A_{cr}$	Gel effect critical point parameter	9.44	$(\text{kg/mol})^{0.5}$	[28]
$A_l$	Gel effect testing parameter	0.348	—	[28]
$B$	Glass effect tuning parameter	1.00	—	[28]
$C$	Cage effect tuning parameter	1.00	—	[28]
$E_{cr}$	Gel effect critical point exponent parameter	1.60e4	J/mol	[28]
$E_d$	Chemical initiation activation energy, DCP	1.53e5	J/mol	[28]
$E_{dm}$	Thermal initiation activation energy	1.16e5	J/mol	[11]
$E_p$	Propagation activation energy	3.25e4	J/mol	[28]
$E_{tc}$	Termination activation energy	1.40e4	J/mol	[28]
$E_{trM}$	Transfer to monomer activation energy	1.27e5	J/mol	[28]
$f$	Initiator efficiency	0.85	—	—
$k_{d,0}$	Chemical initiation frequency factor, DCP	9.24e15	1/s	[28]
$k_{dm,0}$	Thermal initiation frequency factor	0.219	$\text{m}^6/\text{mol}^2 \cdot \text{s}$	[11]
$k_{p,0}$	Propagation frequency factor	4.27e4	$\text{m}^3/\text{mol} \cdot \text{s}$	[28]
$k_{tc,0}$	Termination frequency factor	1.47e7	$\text{m}^3/\text{mol} \cdot \text{s}$	[28]
$k_{trd,max}$	Reaction diffusion maximum bound	1.74e-27	—	[28]
$k_{trd,min}$	Reaction diffusion minimum bound	2.34e-26	—	[28]
$k_{trM,0}$	Transfer to monomer frequency factor	6.05e12	$\text{m}^3/\text{mol} \cdot \text{s}$	[28]
$R$	Gas constant	8.314	J/molK	—
$T_{g,C5}$	Glass transition temperature, pentane	123	K	[28]
$T_{g,M}$	Glass transition temperature, monomer	185	K	[28]
$T_{g,P}$	Glass transition temperature, polymer	370	K	[28]
$V_{f,cr,d}$	Critical free volume for cage effect onset	0.069	—	[28]
$V_{f,cr,p}$	Critical free volume for glass effect onset	0.0465	—	[28]
$W_{ag}$	Agitation work	500	W/m <sup>3</sup>	—
$\alpha_{C5}$	Fractional free volume for pentane	0.00079	—	[28]
$\alpha_M$	Fractional free volume for monomer	0.001	—	[28]
$\alpha_P$	Fractional free volume for polymer	0.00028	—	[28]
$\delta_c$	Segmental diffusion parameter	0.001	—	[28]
$\Delta H_R$	Reaction enthalpy	-7.11e4	J/mol	[11]
$\rho_{C5}$	Density of pentane	$649 - 1.15(T_R - T_0)$	kg/m <sup>3</sup>	[37]
$\rho_I$	Density of initiator, DCP	1560.00	kg/m <sup>3</sup>	[43]
$\rho_M$	Density of styrene	$924.0 - 0.918(T_R - T_0)$	kg/m <sup>3</sup>	[44]
$\rho_P$	Density of polystyrene	$1084.8 - 0.605(T_R - T_0)$	kg/m <sup>3</sup>	[44]
$\rho_W$	Density of water	1000.00	kg/m <sup>3</sup>	—

## B Optimization of Monomer to Initiator Ratio and Temperature Profile with High Cooling Water Temperature

Figures B.1-B.3 show the results from optimization of the monomer to initiator ratio and temperature profile using a constant cooling water temperature of 20 °C. This could for instance be the water temperature of a river in the summer.

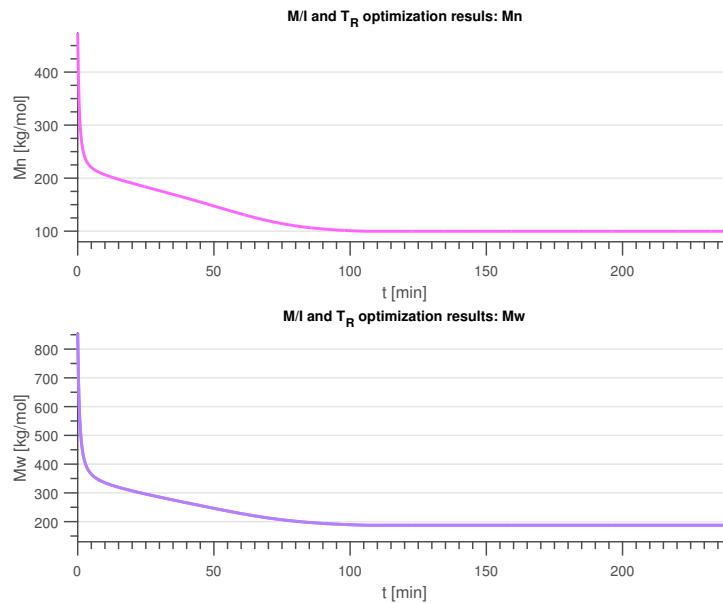


**Figure B.1:** Number and weight average molecular weights for monomer to initiator ratio and temperature profile optimization.

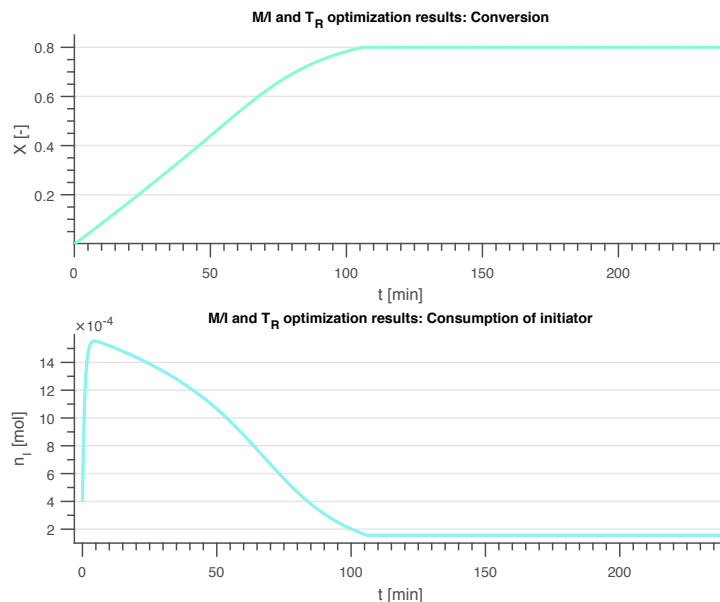


**Figure B.2:** Styrene conversion and initiator consumption for monomer to initiator ratio and temperature profile optimization.

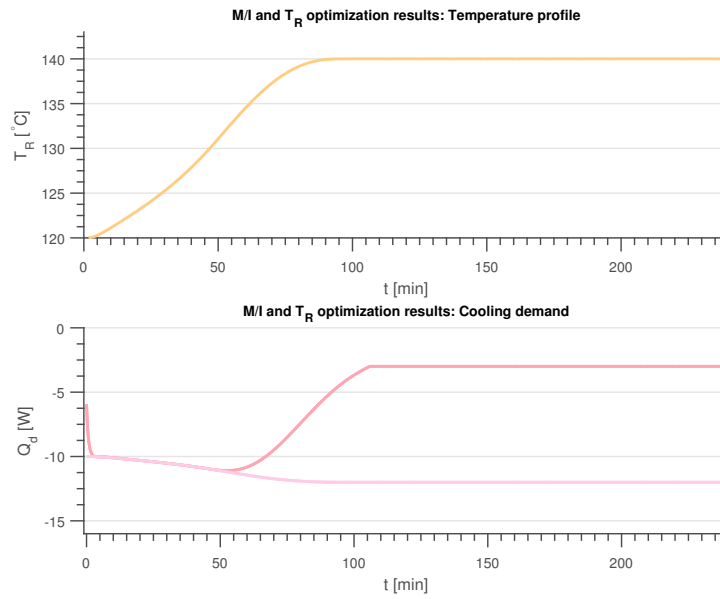


**Figure B.3:** Temperature profile and cooling demand for monomer to initiator ratio and temperature profile optimization.

The end product number average molecular weight is 99.8 and the corresponding value for the weight average molecular weight is 187.59. The optimal monomer to initiator ratio was calculated to be 625, and the temperature varies from  $T_{R,0} = 120.1^\circ\text{C}$  and the maximum temperature of  $140.0^\circ\text{C}$ . These conditions result in a batch time of 106.4 min.